Involvement of hippocampal subfields and anterior-posterior subregions in encoding and retrieval of item, spatial, and associative memories: Longitudinal versus transverse axis.

Stanislau Hrybouski[1,a], Melanie MacGillivray[1,a], Yushan Huang[2], Christopher R. Madan[3], Rawle Carter[2], Peter Seres[2], Nikolai V. Malykhin[1,2]*.

[1]Neuroscience and Mental Health Institute, [2]Department of Biomedical Engineering, University of Alberta, Edmonton, Alberta, Canada; [3]School of Psychology, University of Nottingham, Nottingham, United Kingdom.

*Corresponding author, [a] Shared first authorship.

Nikolai V. Malykhin M.D., Ph.D., Department of Biomedical Engineering, Faculty of Medicine & Dentistry, University of Alberta, Edmonton, Alberta, Canada, T6G 2V2 Phone: (780) 248-1120 Fax: (780) 492-8259, nikolai@ualberta.ca

ABSTRACT

The functional role of the hippocampal formation in episodic memory has been studied using functional magnetic resonance imaging (fMRI) for many years. The hippocampus can be segmented into three major anteroposterior sections, called head, body and tail, and into the *Cornu Ammonis* (CA), dentate gyrus (DG), and subiculum (Sub) subfields based on its transverse axis. However, the exact role of these subregions and subfields in memory processes is less understood. In the present study we combined ultra-high resolution structural Magnetic Resonance Imaging (MRI) at 4.7 T with an event-related high-resolution fMRI paradigm based on the 'Designs' subtest of the Wechsler Memory Scale to investigate how the hippocampal subfields and longitudinal subregions are involved in encoding and retrieval of item, spatial, and associative memories. Our results showed that during memory encoding, regardless of the type of memory being learned, all subregions and all subfields were active. During the retrieval phase, on the other hand, we observed an anterior to posterior gradient in hippocampal activity for all subfields and all types of memory. Our findings also confirmed presence of an anterior to posterior gradient in hippocampal activity during spatial learning. Comparing subfield activities to each other revealed that the DG was more active than the CA1-3 and Sub during both encoding and retrieval. Finally, our results showed that for every subfield, encoding vs. retrieval activity differences were larger in the hippocampal head than in the hippocampal body and tail. Furthermore, these encoding vs. retrieval activity differences were similar in all subfields, highlighting the importance of studying both the longitudinal and transverse axis specialization simultaneously. Current findings further elucidate the structure–function relationship between the human hippocampus and episodic memory.

Highlights

- Hippocampus responded similarly during item, spatial, and associative learning

- The entire hippocampus was active during memory encoding

- Retrieval activity was characterized by an anterior to posterior gradient

- Dentate gyrus showed the largest BOLD activity during both encoding and retrieval

- Both the longitudinal and transverse properties characterize hippocampal function

Keywords

High-resolution fMRI, hippocampal subregions, hippocampal subfields, episodic memory, dentate gyrus, cornu ammonis.

INTRODUCTION

For over fifty years the hippocampus (HC) has been a major source of scientific interest because of its role in establishing and supporting episodic memories (Eichenbaum, 2001; Scoville & Milner, 1957; Squire & Dede, 2015; Squire & Wixted, 2011). Extensive research into HC function in both animals and humans confirmed the HC role in numerous components of episodic memory, including content, spatial, and temporal information (for reviews, see Cohen et al., 1999; Lisman et al., 2017; Moscovitch et al., 2005, 2016; Squire et al., 2015).

In humans, the HC activity was reported during both explicit and incidental learning (Azab et al., 2014; Bakker et al., 2008; Cohen et al. 1999; Lacy et al., 2011; Ranganath et al., 2004) with a wide variety of stimuli, covering a broad set of cognitive and perceptual domains: words, objects, tones, scenes, faces, and spatial routes and landmarks (for overview, see Cohen et al., 1999; Lisman et al., 2017). From these studies, various hypotheses of HC function emerged: novelty detection, cognitive mapping, pattern separation/completion, and relational memory (Cohen et al., 1999; Cohen & Eichenbaum, 1993; Lisman et al., 2017; Yassa & Stark, 2011).

To gain a more accurate understanding of the HC function, it is important to acknowledge its complex internal anatomy. The HC can be subdivided along the anterior-posterior axis into three major sections (sometimes called subregions): head, body and tail (Duvernoy, 2005; Malykhin et al., 2007; Rajah et al. 2010). Although functional differences between the anterior (i.e., head) and posterior (i.e., body together with tail) HC have been discovered, the exact nature of these differences is still unknown (Poppenk et al., 2013; Small, 2002; Strange et al., 2014). For instance, a number of studies demonstrated that the posterior HC is active during spatial memory

tasks, while the anterior HC is engaged if a memory task contains emotional information (Bannerman et al., 2004; Dolcos et al., 2004; Kensinger & Corkin, 2004; Kensinger, 2009; Strange et al., 2014; Poppenk & Moscovitch, 2011). It has also been suggested that the anterior HC is related to coarse gist-like memory, while the posterior HC is particularly involved in detailed episodic memory (Bonne et al., 2008; Hayes, et a., 2011; Poppenk and Moscovitch, 2011; Poppenk et al., 2008, 2013). Yet other work has shown that the anterior HC is specialized for memory encoding, while the posterior HC is critical for memory retrieval (Kim, 2015; Lepage et al., 1998; Schacter & Wagner, 1999; Spaniol et al., 2009; de Vanssay-Maigne et al., 2011, Woollet & Maguire, 2012; Woollett et al., 2009). However, encoding and retrieval processes were oftentimes studied separately, using memory paradigms unrelated to standardized neuropsychological batteries commonly used for memory assessment in clinical populations. Furthermore, most studies of the HC long-axis specialization did not separate the HC body from the HC tail, and as a consequence, it is currently unclear whether these two subregions perform similar functions (Poppenk et al., 2013; Small, 2002).

Anatomical connectivity studies suggest that splitting the HC into just two (i.e., anterior and posterior) sections might lead to oversimplified models of its function (Small et al., 2002; Strange et al. 2014). Due to differences in sensory input, it has been proposed that the long axis is organized along a gradient (Poppenk et al., 2013), with the intermediate HC serving as a key interface point between spatial encoding and behavioral control systems (Strange et al., 2014). Based on anatomical connectivity profiles of different HC segments, Small et al. (2002) proposed three functionally distinct segments within the HC: anterior, middle, and posterior. Consistent with this notion, a series of volumetric and functional experiments revealed that the HC head, body, and tail might play unique roles in memory (Chen et al., 2010; DeMaster et al.,

4

2014; Evensmoen et al., 2013; Spalletta et al., 2016; Travis et al, 2014; de Vanssay-Maigne et al. 2011), while a growing body of clinical MRI literature suggests that different pathological processes sometimes affect the HC head, sometimes the HC body, and sometimes the HC tail (Bouchard et al. 2008; Elliott et al., 2016; Frisoni et al., 2008; Huang et al., 2013; Lindberg et al., 2012; Maller et al. 2007, 2012; Malykhin et al., 2017; Spalletta et al., 2016; Vassilopoulou et al., 2013).

Aside from studying functional differences along the HC anterior-posterior axis, recent advances in functional Magnetic Resonance Imaging (fMRI) enabled researchers to study functional implications of its cross-sectional subfields (transverse axis): *Cornu Ammonis 1-3* (CA1-3), dentate gyrus (DG) and subiculum (Sub) (Aly et al., 2016; Azab et al., 2014; Bakker et al., 2008; Berron et al., 2016; Bonnici et al., 2012; Copara et al., 2014; Duncan et al., 2012; Eldridge et al., 2005; Lacy et al., 2011; Reagh et al., 2014; Stokes et al., 2015; Suthana et al., 2009, 2011, 2015; Tompary et al., 2016; Yassa & Stark, 2011; Zeineh et al., 2003). Because of technical limitations, many of these studies did not segment subfields within the entirety of the HC head (Chen et al., 2011; Copara et al., 2014; Eldridge et al., 2005; Nauer et al., 2015; Stokes et al., 2015; Suthana et al., 2009, 2011; Zeineh et al., 2003) or tail (Berron et al., 2016; Chen et al., 2011; Eldridge et al., 2005; Zeineh et al., 2003), producing activity estimates heavily dominated by the signal from the HC body. Furthermore, while many studies report sub-millimeter in-plane resolution for their subfield segmentations, these were oftentimes collected with relatively thick (i.e, >1.5 mm) slices (Copara et al., 2014; Eldridge et al., 2005; Suthana et al., 2009, 2011, 2015; Stokes et al., 2015; Zeineh et al., 2003). In general, sufficient contrast for subfield segmentation in the most anterior and posterior segments of the HC formation is obtained with slice thickness of 1 mm or less (Bonnici et al., 2012; Malykhin et al., 2010, 2017; Winterburn, et

al. 2014; Wisse et al., 2012); however, several studies (e.g., La Joie et al., 2010; Yushkevich et al., 2015b) managed to segment subfields within the HC head and tail on T2-weighted MRI data with 2-mm thick slices. Finally, most of the aforementioned subfield studies relied on either some form of voxel-wise hypothesis testing (which can be vulnerable to Type-II error due to strict correction for multiple comparisons, further compounded by small sample sizes of 10-20 participants in most fMRI studies of the HC subfields) or performed region of interest (ROI) analyses on subfields, collapsed across the entire long-axis coverage, potentially oversimplifying the HC anatomy and its relationship to memory. It is currently unclear whether it is the longitudinal or the transverse axis or the interaction between the two that best explains the HC role in episodic memory.

In addition, there is a lack of consensus in the HC literature as to whether the HC formation is dedicated to processing of spatial vs. non-spatial components of episodic memory (Eichenbaum, 2017; Eichenbaum & Cohen, 2014; Kumaran & Maguire, 2005; Lisman et al., 2017; Nadel et al., 2012), and whether the HC is involved in item, not just relational memory (Davachi et al., 2003; Gold et al, 2006; Konkel et al., 2008). In our previous structural MRI study (Travis et al., 2014), we showed that performance on the 'Designs' subtest of the Wechsler Memory Scale (WMS-IV; Pearson Education Inc., 2009) was correlated with volumes of the posterior CA1-3 and DG subfields. This particular subtest was designed to test performance on item, spatial, and item-location associative memory. Despite widespread clinical use of the WMS-IV since its inception in 2009, little research has been done on the 'Designs' subtest other than the initial validation study (Martin and Schroeder, 2014). Although our earlier structural work (Travis et al., 2014) provides some insight into how the WMS-IV 'Designs' subtest relates to the HC neuroanatomy, volumetric measurements are crude proxies for brain function and cannot truly explain how

6

processes underlying formation and retrieval of item, spatial, and associative memories (assessed by this task) relate to metabolic activity in various segments of the HC structure. Consequently, the main goal of this study was to investigate how activity in various HC subfields and long-axis subregions relates to both encoding and retrieval processes for item, spatial, and associative memories in a 'Designs'-like paradigm, within a single fMRI experiment. To answer these questions, we administered a computerized adaptation of the WMS-IV 'Designs' subtest and used high-resolution fMRI methods in conjunction with manual delineation of the HC subfields within the entire HC formation on ultra-high resolution structural MRI.

Since multiple theories of HC function (for overview, see Poppenk et al., 2013) suggest that the posterior HC should be more active during retrieval of detailed memories, we expected to see greater involvement of the posterior HC in retrieval processes. Second, we expected preferential engagement of the posterior HC subfields on spatial memory trials, while item and associative memory trials would not show longitudinal differences in HC activity. Furthermore, we hypothesized that longitudinal differences are not a sharp dichotomy and are best represented by a linear head to tail gradient (Kim, 2015; Poppenk et al., 2013; Small et al., 2002; Strange et al. 2014). Lastly, based on our previous volumetric study (Travis et al., 2014) we predicted that the posterior DG and CA1-3 subfields play a critical role in the 'Designs' subtest. To additionally improve accuracy and validity of our HC BOLD response measurements, we used a multi-parameter hemodynamic response deconvolution procedure, aimed at minimizing assumptions about neural and vascular responses during different phases of our memory task.

MATERIALS AND METHODS

Participants

Twenty-five healthy individuals (12 males, 13 females, mean age = 25.4 years, range 20-33, mainly graduate and undergraduate students attending the University of Alberta) were recruited through online and poster advertisements. All participants were right-handed with no reported personal history of psychiatric or neurological illness, and drug or alcohol abuse as assessed by a structured interview (Anxiety Disorders Interview Schedule-IV; Brown et al., 2001). The exclusion criteria were active and inactive medical conditions that may interfere with normal cognitive function and use of medication and non-prescribed substances that could affect brain function. Written, informed consent was obtained from each participant. The study protocol was approved by the University of Alberta Health Research Ethics Board.

Memory task

Our memory task was based on the "Designs" subtest of the Wechsler Memory Scale (WMS-IV; Pearson Education Inc., 2009). The 'Designs' subtest is a highly flexible tool of assessing item, spatial, and item-location binding simultaneously. During the "Designs" test, an examiner shows the examinee a grid containing 4-8 abstract symbols within a 4×4 grid for 10 s. Episodic memory is tested after a brief ($\approx$5 s) break in two different ways: the examinee (1) re-creates the grid by choosing the abstract symbols they remember and placing them in the corresponding locations, and (2) by performing spatial pattern recognition.

However, when administering the WMS-IV, each examinee is presented with only 4 grids, a number of trials that is insufficient for event-related fMRI. To increase the number of potential grids for our fMRI paradigm, we included additional symbols not only from the "Designs," but also from the "Symbol Span" subtest. Abstract symbols from the 'Designs' and 'Symbol Span'

subtests were scanned from a paper version of the WMS-IV and resampled to a 700×500 pixel resolution. Next, a single rater (MM) generated 11 categories broadly summarizing symbols' patterns, and categorized each symbol accordingly (e.g., arrow-like, XX-shaped). Symbol classification was performed to ensure that all symbols within each fMRI trial were sufficiently distinct: only one symbol from a given category could appear on the same grid during encoding or retrieval.

Experimental design

Similar to the "Designs" subtest of the WMS-IV, each trial in our paradigm consisted of one encoding and one retrieval phase. Between the encoding and retrieval trials an odd/even judgment task (one judgment every 1.25 s) was performed in place of passive fixation. Performing odd/even judgments between the two task phases not only limits rote rehearsal, but also produces more accurate estimates of memory-related BOLD activation, particularly inside the HC formation (Stark & Squire, 2001). All odd/even inter-stimulus-intervals ISIs, which separated the encoding and retrieval phases from each other, were randomized on a negative exponential distribution with a median of 12.5 s and lasted between 7.5 and 20.0 seconds.

During the encoding phase, participants studied 4×4 horizontal grids, each containing four abstract symbols randomly placed in 4 out 16 possible cells. Each trial began with one of three cues: 'S' for Symbol, 'L' for location, and 'B' for both. The 'S' cue instructed participants to prioritize symbol learning, regardless of their positions inside the grid (see Fig. 1a). The 'L' cue instructed the participants to remember which cells in the grid contained a symbol, regardless of which symbols were present in those cells. The 'B' cue instructed the participants to learn symbol-location associations. Recent work by Aly and Turk-Browne (2016) demonstrated that HC activity is modulated by attention and that this modulation is stable across various stimuli as

9

long as attention is maintained on a particular type of information within a stimulus. Our design leveraged this finding: during encoding we manipulated attention, as opposed to the stimuli themselves, guaranteeing that any encoding-related activity differences within the HC, when comparing item, location, and associative memories to each other, would be unrelated to visual properties of the stimuli themselves.

Participants' memories were tested in accordance with the previous cue on 2 (out of 4) randomly chosen items. If 'S' was the encoding cue, participants completed symbol recognition: they saw four symbols on a screen for 5 s, only one of which was present in the previously studied grid (Fig. 1b). To decouple memory retrieval from motor planning, response cues (randomly placed numbers corresponding to MR-compatible button presses) were presented only for the last 3 s of each recognition test. If 'L' served as the encoding cue, participants completed a location recognition task, during which they saw a blank 4×4 grid for 2 seconds. Subsequently, numbers 1 to 4 (corresponding to MR button presses) appeared in 4 cells. Only one of those cells contained a symbol in the previously studied grid (Fig. 1c). Finally, if 'B' was the encoding cue, participants performed one of two versions of a cued recall task (Fig. 1d-e). In the first version, grid locations were used as cues, and participants were instructed to identify which symbol was shown in a cued location during the previous encoding phase (Fig. 1d). In the second version, symbols were used as cues, and participants were asked to identify in which location on the grid a cued symbol was initially placed (Fig. 1e).

To ensure that participants were familiar with the task and the button-press response system, they completed in-scanner button-press training, odd/even judgment training, and one practice run with immediate accuracy feedback while the scanner was undergoing calibration procedures. In total, there were 12 task runs, each lasting 155 s, with three trials in each run: one set of symbol,

location, and both in randomized order. All encoding trials lasted 10 s, regardless of the encoding cue. The retrieval sessions for the symbol and location conditions lasted 10.5 s, and 14.5 s for the association condition. In addition, for the association condition, 6 trials tested memory by providing symbols as cues, and 6 trials tested memory by providing grid locations as cues, in random order for each participant. To establish the fMRI baseline and to capture the hemodynamic response for the final memory trial, each run began with 6.25 s and ended with 11.25 s of the odd/even judgment task. Our task was programmed in Python-based software PsychoPy (Peirce, 2007, 2009), and was displayed inside the scanner through an MR-compatible 1080p 32" LCD panel (Cambridge Research Systems Ltd., Rochester, UK).

MRI data acquisition

All images were acquired on a 4.7 T Varian Inova MRI scanner at the Peter S. Allen MR Research Centre (University of Alberta, Edmonton, AB) using a single-transmit volume head coil (XL Resonance) with a 4-channel receiver coil (Pulseteq). 744 functional volumes were collected axially (in parallel to the AC–PC line) over 12 runs using a custom-written T2*-sensitive Gradient Echo Planar Imaging (EPI) pulse sequence [repetition time (TR): 2500 ms; echo time (TE): 19 ms; flip angle: 75°; field of view (FOV): 168×210 mm^2; voxel size: $1.5 \times 1.5 \times 1.4$ mm^3; inter-slice gap: 0.1 mm; 35 slices acquired sequentially; GRAPPA parallel imaging with in-plane acceleration factor 2 (Griswold et al., 2002)]. For the HC subfield and subregion segmentation, high-resolution coronal structural images were acquired perpendicular to the AC–PC orientation using a custom-written T2-weighted 2D Fast Spin Echo (FSE) sequence [TR: 11000 ms; TE: 39 ms; FOV: 200×200 mm^2; voxel size: $0.52 \times 0.68 \times 1.0$ mm^3; 90 slices]. To improve image registration accuracy between the anatomical scans and the functional scans axial high-resolution 2D FSE images were acquired with a coverage closely

matching the fMRI data [TR: 7000 ms; TE: 38 ms; FOV: 210×200 mm^2; voxel size: $0.52 \times 0.68 \times 1.0$ mm^3; 45 slices]. A whole brain T1-weighted 3D Magnetization Prepared Rapid Gradient-Echo (MPRAGE) sequence [TR: 8.5 ms; TE: 4.5 ms; inversion time: 300 ms; flip angle: 10°; FOV: $256 \times 200 \times 180$ mm^3; voxel size: $1 \times 1 \times 1$ mm^3] was used to acquire anatomical images for automatic tissue segmentation. Finally, to correct for inhomogeneity-related EPI distortions, we used a multi-echo 3D gradient echo sequence [TR: 577.8 ms; TE: 3.56, 6.71 ms; flip angle: 50°; FOV: 192 x 168 mm^2; voxel size: $1.5 \times 1.5 \times 1.5$ mm^3; 35 slices] to calculate B$_0$ fieldmap for each participant. The entire image acquisition was spread over two separate sessions, at most two weeks apart. Coronal FSE images and whole-brain MPRAGE images were acquired during the first (1 hour) visit, while the fMRI data, along with Axial FSE, and fieldmaps were collected during the second (1.5 h) visit. During the fMRI session, we also collected cardiac and respiration waveforms using an MP150 system with a pulse photoplethysmograph placed on the left ring finger and a pneumatic belt strapped around the upper abdomen, respectively (Biopac Systems Inc., Montreal, QC). Fig. 2 demonstrates orientation and brain tissue coverage for structural and functional data.

Hippocampal segmentation

All HC ROIs were manually traced on the T2-weighted coronal FSE images with a mouse-driven cursor using freely available FreeView v. 4.0 software (MGH, Boston, MA), while ITK-SNAP (v. 3.6.0; Yushkevich et al., 2006) was used to construct 3D models of the HC ROIs on data from one participant for visual demonstration (see Fig. 3). Our subfield segmentation technique (Malykhin et al., 2010) was developed with the guidance from the Duvernoy's (2005) atlas of the human HC and is based on structural connectivity, as opposed to cytoarchitectonic properties.

Here, we divided the HC into three subfield areas corresponding to our best approximation of the CA areas 1-3 (CA1-3), DG&CA4 (henceforth referred to as DG), and Sub within the HC head, body, and tail (Malykhin et al., 2007, 2010). In our parcellation method the most posterior coronal slice of the HC head was the first slice where the uncal apex (uncus) was clearly present (Duvernoy, 2005). The most anterior coronal slice of the HC body slice was the slice just before the appearance of uncus (Malykhin et al., 2007, 2010). The most anterior coronal slice of the HC tail was the first slice where the fornix was clearly seen in full profile, or was separated from the wall of the ventricle, whichever came first (Malykhin et al., 2007, 2010). Similar definitions of the long-axis subregions have been used by other studies with MRI acquisitions perpendicular to the AC-PC axis (Boccardi et al., 2015; Malykhin et al., 2007, 2010; Pruessner et al., 2000), as well as by studies with MRI acquisition perpendicular to the HC longitudinal axis (Daugherty et al., 2015; La Joie et al., 2010). Because a substantial portion of the CA3 subfield is encapsulated within the DG/CA4 on coronal slices (Adler et al., 2014; Ding & Van Hoesen, 2015), it is virtually impossible to separate the CA3 from the DG ROIs based on image contrast alone (Reagh et al., 2014). As a result the CA3 subfield in our segmentations was almost evenly split between the DG and CA1-3 ROIs (Malykhin et al., 2010), while the CA2 subfield was fully integrated into the CA1-3 ROI. Furthermore, our Sub volumes consisted predominantly of the Sub proper, and excluded most of the presubiculum or parasubiculum.

All segmentations of the HC subregions (head, body & tail) and HC subfields (CA1-3, DG & SUB) were performed by a single highly experienced rater (YH), trained by the developer of the protocol (NM). Intra-rater and inter-rater reliabilities for the HC subfield/subregion volumes were assessed by retracing structural T2-weighted MRI images from 5 subjects (i.e., 10 HC total) at a one-week interval. Inter/intra-rater reliability intraclass correlation coefficients (ICCs) for

the long-axis subregions were as follows: 0.95/0.92 for the HC head, 0.83/0.93 for the HC body and 0.95/0.88 for the HC tail. The corresponding inter/intra-rater Dice similarity coefficients (DSCs) were 0.89/0.90 for the HC head, 0.86/0.87 for the HC body, and 0.80/0.82 for the HC tail. For the cross-sectional subfields, the inter/intra-rater reliability ICCs were as follows: 0.92/0.92 for the CA1-3, 0.86/0.84 for the DG, and 0.87/0.95 for the Sub. Matching inter/intra-rater DSCs were 0.73/0.75 for the CA1-3, 0.81/0.81 for the DG, and 0.74/0.74 for the Sub. For the total HC segmentations inter/intra-rate ICCs were 0.95/0.97, and inter/intra-rater DSCs were 0.89/0.90. Furthermore, each of the aforementioned ICCs was statistically significant at $\alpha = .001$. Following manual segmentation on structural MRI, all HC labels were down-sampled (using nearest neighbor interpolation) to match the resolution of fMRI acquisition. Next, a single rater (YH) manually adjusted all ROIs to ensure accurate overlap between the original labels and the downsampled ones and to remove all ROI voxels severely impacted by susceptibility artifacts. Since individual subfield volumes (particularly Sub) within the HC tail are very small when resampled to fMRI resolution (see Table 1 for ROI volumes), we merged subfields from the HC body with those from the HC tail. This reduced volumetric discrepancies between subfield ROIs and improved temporal signal-to-noise ratio (tSNR) in smaller subfields (see Table 2 for tSNR details). However, to verify that activity in the HC body was indeed similar to that in the HC tail, we also analyzed activity in each long-axis subregion separately. Fig. 3 demonstrates our segmentation methodology on structural and functional data.

Image preprocessing

Most of the image processing was performed in SPM12 (Wellcome Trust Centre for Neuroimaging, UCL, UK). Prior to registration, MPRAGE images underwent correction for intensity non-uniformity using N3 program (Sled et al., 1998). Next, anatomical images were

cropped using custom-written MATLAB code (The MathWorks Inc., Natick, MA) to isolate areas of overlapping coverage. These overlapping portions of anatomical images were used to compute rigid-body transformation matrices to register all anatomical images to each other.

Unified '*realign & unwarp*' function in spm12 was used to correct geometric distortions in fMRI data caused by B_0 inhomogeneity and to realign all fMRI volumes to the first functional volume (Andersson et al., 2001). Next, an average EPI was computed and was registered to the axial FSE image using a combination of manual and automatic registration tools. To ensure optimal registration for the HC formation, white matter (WM)/grey matter (GM) boundaries were (manually traced on three coronal, three axial, and three sagittal slices proximal to the HC) used to fine-tune image alignment. Automated rigid-body registration tools were then used to register all the remaining fMRI volumes to the manually registered average EPI volume. To identify signal spikes and to account for spin-history-related head-movement artifacts in the fMRI time series, we used Artifact Detection Toolbox (ART; http://www.nitrc.org/projects/artifact_detect/) for MATLAB. All fMRI volumes with framewise displacement > 0.5 mm/TR were marked for scrubbing, as were all fMRI volumes with noticeable signal spikes (i.e., scan-to-scan differences in signal intensity > 3 SDs above the run's mean). Because we employed sequential slice acquisition, the most superior and the most inferior slices with HC were acquired less than 1.25 s apart in most participants. Rather than risk artifacts caused by slice timing correction, we ensured that all HRf-related regressors during GLM parameter estimation were temporally aligned to acquisition of the middle HC slice in each subject. Similarly, in order to preserve spatial resolution no spatial smoothing was applied to the fMRI data.

Physiological noise correction was performed using custom-written MATLAB implementation of RETROICOR (Glover, et al., 2000) and RVTHR techniques (Birn et al., 2006, 2008; Chang et

al., 2009). From cardiac waveforms, we created 12 nuisance regressors to absorb signal changes due to blood flow pulsatility (RETROICOR 2nd-order Fourier basis, temporally aligned to acquisition of the most superior, middle HC, and most inferior slices of each fMRI volume) and one regressor to absorb signal changes due to heart rate variability (Chang et al., 2009; Glover et al., 2000). Each participant's respiratory waveforms were used to generate 4 respiratory regressors (RETROICOR 2nd-order Fourier basis temporally aligned to acquisition of the middle HC slice, t_{TR}), accounting for respiration-induced magnetic field changes (Glover et al., 2000), as well as 3 time-lagged [$t_{TR} - 8$ s, $t_{TR} - 2$ s, $t_{TR} + 4$ s] regressors representing respiratory volume per time (RVT) convolved with the respiratory response function (Birn et al., 2008). Those three RVT-related regressors were used to absorb variability in the fMRI time series caused by fluctuations in CO_2 concentration resulting from variation in breath depth and/or breath rate (Birn et al., 2006, 2008). Next, we generated a partially filtered fMRI dataset, from which motion, cardiac respiratory signals, and low frequency signal drifts (128 s high-pass filter) were removed. From this dataset the first three eigenvariate WM time courses and the first three eigenvariate CSF time courses were extracted using preprocessing functions implemented in CONN toolbox for MATLAB (v. 16.a; Whitfield-Gabrieli & Nieto-Castanon, 2012). In total, for each fMRI run, there were 32 nuisance regressors (20 RETROICOR&RVTHR, 6 WM&CSF, and 6 motion from realignment), plus one regressor for each fMRI volume marked for scrubbing based on movement and global signal intensity criteria described above. In all GLM procedures, low frequency signal drifts were removed with a 128 s high-pass filter, and first order autoregressive (AR1) correction for serial autocorrelation was applied.

Estimation of hemodynamic response functions for encoding and retrieval

The profile of the hemodynamic response function (HRf) in subcortical brain regions need not be the same as the standard double-gamma function often used to model cortical responses

16

(Devonshire et al., 2012; Ekstrom, 2010; Handwerker et al., 2004; Hrybouski et al, 2016; Pernet, 2014). Consequently, extracting raw signal change over points in time without reference to a standard hemodynamic template often leads to more accurate BOLD signal measurements. While it is well established that FIR-based approaches provide more accurate depictions of BOLD response (Glover, 1999; Lindquist et al., 2009) as they make no assumption about neural or vascular properties of a region (FIR basis set contains one free parameter for every time point in every trial type) FIR deconvolution can produce noisy solutions in typical fMRI datasets (Goutte et al., 2000; Lindquist et al., 2009). Similar to our previous high-resolution fMRI work (Hrybouski et al., 2016), we incorporated methodology designed to minimize the HRf bias without substantial loss of statistical power by computing task- and region-specific double-gamma functions for activation analyses.

First, the HC HRf was deconvolved using the FIR technique (8 TR bins). Events for all stimuli categories ('S', 'L', and 'B') were pooled together, regardless of subsequent memory performance, and the mean HRf was estimated for each HC, separately for encoding and retrieval phases. These FIR results revealed that the informed basis set (i.e., canonical HRf with time and dispersion derivatives) would be sufficient to estimate the HC HRf in our task. Consequently, we used the informed basis set model to deconvolve the HRf for each event for each condition separately (encoding 'S', encoding 'L', encoding 'B', retrieval 'S', retrieval 'L', and retrieval 'B'). The HRf and derivative betas were used to reconstruct task-related signal change for each event. It is worth noting that this approach treats the derivative betas as BOLD response modulators rather than covariates (Calhoun et al., 2004; Henson et al., 2002; Hrybouski et al., 2016). Because the ISI between the retrieval tests was short (0.5 s), and did not vary from trial to trial, it was not feasible to deconvolve BOLD signal for individual retrieval tests. Instead,

we restricted all activity analyses to trials for which participants obtained 2 out 2 retrieval accuracy: 11.12 (SD = 0.97) trials for the symbol condition, 8.40 (SD = 2.36) trials for the location condition, and 8.00 (SD = 2.06) trials for the association condition, on average. These numbers are substantially higher than what would be expected if subjects were randomly guessing on memory tests [sampling distribution for 2 out 2 retrieval accuracy under the null hypothesis was estimated using 1,000,000 Monte Carlo simulations; mean = 0.75, standard error = 0.17]. By limiting our analyses to trials on which successful learning took place, we eliminated memory-related variability in BOLD signal onset during retrieval and ensured that HC activity estimates during the preceding encoding phase were linked to successful formation of novel memories. The latter is particularly important as prior fMRI studies demonstrated differential encoding activity for remembered vs. forgotten stimuli (Chua et al., 2007; Gold et al., 2006; Ranganath et al., 2004).

Subsequently, subject-specific encoding and retrieval HRf time courses were estimated for each left/right HC ROI (i.e., total HC, total head, total body, total tail, total CA1-3, total DG, total Sub, head CA1-3, head DG, etc.), separately for each memory condition (i.e., symbols, locations, both). Using this approach, we obtained 96 encoding and 96 retrieval HRfs from each subject. These HRfs were then rescaled to % signal change units and averaged across participants. Next, each of the 192 (96 encoding, 96 retrieval) subject-averaged HRf time courses was manually classified by a single observer (SH) as being (1) BOLD-like activations, (2) BOLD-like deactivations, or (3) noise. The following rules, developed based on previously published neurovascular coupling literature (Glover, 1999; Goutte et al., 2000; Lindquist et al., 2009; Logothetis et al., 2001; Shmuel et al., 2006) were used to perform this HRf labeling:

1. *Reconstructed response must be non-linear with initial increase (or decrease for deactivation) in signal, followed by a peak (or trough for deactivation) with a subsequent return to the baseline. The informed basis set, which was used to estimate HRfs in this study, enforces zero baseline prior to stimulus onset and ~ 16 s after stimulus onset. HRfs showing consistent increases or decreases in activity were classified as noise.*

2. *At least one clear positive or negative peak is present. Time gap between stimulus onset and HRf peak (or trough) must be at least 3.5 s (~ 2nd poststimulus TR in our study). Whether HRf activity was sustained (i.e., a plateau) or peaked and quickly returned to the zero baseline was irrelevant for classification purposes.*

3. *For BOLD classification, the absolute (relative to the zero baseline) value of the largest peak/trough is greater than the absolute (relative to the zero baseline) value of signal amplitude at first post-stimulus TR; noise classification otherwise.*

4. *(a) If multiple peaks were present, (b) instances when all peaks & troughs were only positive or only negative were classified as BOLD activations or deactivations, respectively. (c) For ambiguous cases with two opposing peaks (i.e., one activation and one deactivation), only HRf cases when the absolute value (relative to the zero baseline) of the larger peak was twice as large as the absolute value (relative to the zero baseline) of the smaller peak were retained (i.e., noise otherwise, as a consequence of poor signal-to-noise ratio), and activation/deactivation labels were assigned in accordance with the sign of the greatest (i.e., dominant) peak/trough.*

5. *Classify BOLD-like (i.e., remaining) HRfs as activation or deactivation. For activation, the largest HRf peak must be above HRf amplitude at the first poststimulus TR. For*

deactivation, the strongest BOLD deactivation must be below the HRf amplitude at the first poststimuls TR.

An algorithmic diagram providing step-by-step instructions on how to classify HRfs using these rules, along with accompanying examples, is available in the Supplementary Materials (Suppl. Fig. 1). Intra-rater and inter-rater classification agreement was assessed by reclassifying 40 randomly chosen HRfs into positive BOLD, negative BOLD, or noise at a one-week interval. Intra-rater reclassification produced the same labels for all 40 HRfs, while inter-rater classification comparison resulted in 97.5% classification agreement between the two raters (SH and NM). Out of 192 HRfs, approximately 15% were categorized as noise, 5% as BOLD deactivation, and the remaining 80% as BOLD activation. All negative BOLD responses were inverted in order to ensure that not only activations, but also deactivations were considered when estimating the optimal overall BOLD response model for the HC formation. Finally, the overall encoding and retrieval HRfs were computed by collapsing positive and inverted negative BOLD responses across HC ROIs and memory conditions. Averaging across task conditions reduces the risk of overfitting the data, especially when comparing HC activity among different memory trials. Similarly, averaging BOLD response across HC ROIs reduces the risk of overfitting a BOLD response model in any particular HC segment, a problem when comparing activity among various HC ROIs. Because of differences in task timing, we did not collapse HRfs across encoding and retrieval phases, and as a result each phase of our memory task had its own empirically-derived HRf. Manual labeling of HRfs in our analysis pipeline took approximately 2 hours to complete.

Next, the SIMPLEX algorithm (Nelder & Mead, 1965) was used to fit double-gamma functions (as implemented in the *spm_hrf* function within SPM) to the average encoding and average

retrieval HRfs. During each fitting procedure, six parameters (delay to response, delay of undershoot, dispersion of response, dispersion of undershoot, ratio of response to undershoot, and onset) were optimized over 20,000 iterations to minimize the root-mean-squared-deviation (RMSD) between the double-gamma function and each of the two HRf time courses. These optimized double-gamma functions (see Fig. 4) were used to model the expected BOLD response for every encoding and retrieval event with 2 out of 2 retrieval accuracy. Our data processing steps are summarized in flow-chart form in Fig. 5.

Lastly, MarsBar toolbox for SPM (v. 0.43; http://marsbar.sourceforge.net) was used to extract beta parameters for each event of interest and to rescale activity estimates to percent signal change units. MarsBar performs ROI-specific scaling, and all rescaled parameters represent signal change in relation to baseline activity. Such scaling procedure is especially relevant to fMRI studies of the HC because, as Olman et al. (2009) showed, anterior HC subfields are more vulnerable to susceptibility artifacts than their posterior counterparts. It is worth noting that in addition to scaling, our acquisition parameters and preprocessing procedures were specifically designed to minimize susceptibility-related confounds when measuring HC activity. Consequently, tSNR differences among various HC segments in our preprocessed fMRI data were less than 15% in most instances (see Table 2 for details).

Statistics

All random-effects analyses were performed in SPSS (v. 22; IBM Inc., Armonk, NY). We statistically compared BOLD activity using four separate ANOVA designs: (1) a two-way repeated-measures ANOVA on total HC activity with participants as a random factor, and Hemisphere (left, right) and Condition (symbol, location, both) as fixed factors; (2) a three-way

repeated-measures ANOVA on total subfields' activity estimates with participants as the random factor, and ROI (CA1-3, DG, Sub), Hemisphere (left, right), and Condition (symbol, location, both) as fixed factors; (3) a three-way repeated-measures ANOVA on total subregions' activity estimates with Total Subregions (head, body, tail) as the ROI factor, and otherwise the same design as in (2); (4) four- and three-way repeated measures ANOVAs, aimed at comparing activities in the anterior (head) and posterior (body + tail) subfields to each other, with Subregion (anterior, posterior), Subfield (CA1-3, DG, Sub), Hemisphere (left, right), and Condition (symbol, location, both) as fixed factors, and participants as the random factor. ANOVAs were first conducted on HC activity during memory encoding, followed by analyses of memory retrieval, and finally on encoding vs. retrieval differences. One-sample t-tests were used to compare HC signal during memory-related processing to baseline activity (i.e., HC activity while performing odd/even judgment task). Holm-Bonferroni correction for multiple hypothesis testing was used for all *post-hoc* comparisons (whether follow-up ANOVAs or t-tests) and for all tests vs. baseline. Only FWE-corrected p-values are reported in the results section. All parametric results were subsequently verified using permutation tests (100,000 shuffles). Since statistical decisions from both approaches were identical, we report GLM-based inferences only.

RESULTS

Behavior

Behavioral results showed that participants performed best during the symbol condition [$M =$ 95.5%; 95% bias-corrected and accelerated (BCa) bootstrap confidence interval (CI) = (93.0%, 97.5%)]. Performance on the more difficult location and association trial types was 79.5% [95%

BCa bootstrap CI = (74.2%, 84.8%)] and 78.3% [95% BCa bootstrap CI = (73.3%, 83.5%)], respectively. We used a one-way repeated-measure ANOVA to compare accuracies across conditions, which revealed a significant main effect of Condition [$F(2,48) = 28.18$, $p < .001$, $\eta^2 = .540$] where performance on the symbol condition was higher than on the location [$t(24) = 6.05$, $p < .001$, $d = 1.21$, $M_{diff} = 16.0\%$] and association [$t(24) = 7.47$, $p < .001$, $d = 1.49$, $M_{diff} = 17.2\%$] conditions. There was no statistical difference in performance between the location and association conditions ($p = .67$).

fMRI: total hippocampus

During memory encoding, there were no differences in activity between conditions in either HC [two-way repeated-measures ANOVA; Condition, $F_{(2,48)} = 0.09$, $p = .91$, partial $\eta^2 = .004$; Condition × Hemisphere interaction, $F_{(2,48)} = 0.78$, $p = .47$, partial $\eta^2 = .031$]. After averaging across trial types, both HC showed increased activity (relative to the odd/even baseline) during memory encoding [Left: $t_{(24)} = 8.00$, $p < .001$; Right: $t_{(24)} = 4.30$, $p < .001$], although activity in the left HC was marginally greater than that in the right HC [$F_{(1,24)} = 3.88$, $p = .060$] (see Fig. 6a, Table 3 for details).

In contrast to the encoding trials, during memory retrieval there were condition-related differences in HC activity [two-way repeated-measures ANOVA; Condition × Hemisphere interaction, $F_{(2,48)} = 9.26$, $p < .001$, partial $\eta^2 = .278$]. In the right HC, activity did not differ between conditions [$F_{(2,48)} = 2.64$, $p = .092$, $\eta^2 = .099$], and after averaging across all trial types, was marginally greater than during odd/even judgment making [$t_{(24)} = 1.98$, $p = .059$]. However within the left HC, we observed condition-related differences in activity [$F_{(2,48)} = 5.63$, $p = .013$, $\eta^2 = .190$], with location trials showing statistically significant deactivation [$t_{(24)} = -3.22$, $p = $

.011], while activity during item and item-location association trials was not statistically different from the odd/even baseline (Table 3). Laterality effects were significant only for the Location condition [$F_{(1,24)}$ = 30.95, $p < .001$] (Fig. 6b). This Condition × Hemisphere interaction was statistically significant in all long-axis segments of the HC formation, and in every subfield (all ps < .050), demonstrating consistent preference of the right HC for spatial memory retrieval.

Both HC were more active during memory encoding than during memory retrieval [left: $t_{(24)}$ = 6.52, $p < .001$; right: $t_{(24)}$ = 2.19, $p = .039$] (Table 3); however, encoding vs. retrieval differential in activity was larger in the left hemisphere [$t_{(24)}$ = 2.58, $p = .016$]. None of the condition-related effects for the encoding vs. retrieval contrast reached statistical significance [two-way repeated-measures ANOVA; Condition, $F_{(2,48)}$ = 0.85, $p = .432$; Condition × Hemisphere interaction, $F_{(2,48)}$ = 2.17, $p = .134$].

fMRI: total hippocampal subfields

Each of the three-way repeated-measures ANOVAs on total subfield data revealed a significant main effect of Subfield [encoding: $F_{(2,48)}$ = 15.98, $p < 10^{-5}$, partial η^2 = .400; retrieval: $F(2,48)$ = 13.54, $p < .001$, partial η^2 = .361; encoding − retrieval: $F_{(2,48)}$ = 4.38, $p = .018$, partial η^2 = .154], while all Subfield-related interactions were not statistically significant (all ps > .10). Consequently, we collapsed all encoding and retrieval data across symbols, locations, and associative trial types and the two hemispheres.

Although all HC subfields were active during encoding trials (see Fig. 7a, Table 3); encoding activity in the DG was larger than in the other two subfields [DG vs. CA1-3: $t_{(24)}$ = 4.51, $p < .001$; DG vs. Sub: $t_{(24)}$ = 5.16, $p < .001$]. Similar to encoding, the DG was more active than the CA1-3 or Sub during memory retrieval [DG Vs. CA1-3: $t_{(24)}$ = 5.75, $p < .001$; DG Vs. Sub: $t_{(24)}$ =

2.91, p = .031]. However, unlike encoding, the DG was the only subfield to show increase in BOLD activity during memory retrieval, when compared to the odd/even judgment task (see Fig. 7b, Table 3). Comparing encoding and retrieval phases to each other revealed that the CA1-3 and DG subfields were more active during memory formation than during memory retrieval [CA1-3: $t_{(24)}$ = 6.54, p < .001; DG: $t_{(24)}$ = 4.34, p < .001], while encoding and retrieval activities in the Sub did not differ from each other (p = .112).

fMRI: total hippocampal subregions

Performing three-way repeated-measures ANOVAs on encoding, retrieval, and encoding vs. retrieval data for the total subregions, did not reveal any significant Subregion × Condition, Subregion × Hemisphere or Subregion × Condition × Hemisphere interactions (all ps > .10). Consequently, as was the case with the total subfields, encoding and retrieval activity estimates for longitudinal subregions were collapsed across hemispheres and trial types.

One sample t-tests showed that all three HC subregions were active during memory encoding [head: $t(24)$ = 3.48, p = .002; body: $t(24)$ = 7.72, p < .001; tail: $t(24)$ = 8.04, p < .001] (see Fig. 7a, Table 3). Although our omnibus ANOVA did not reveal any differences among the HC subregions during memory encoding [$F_{(2,48)}$ = 2.20, p = .122], prior studies suggest presence of an anterior to posterior activity gradient during spatial learning (Colombo et al., 1998; Ryan et al., 2010; Strange et al., 2014; Woollett & Maguire, 2012). To investigate whether our data supported presence of such a gradient, we performed a planned linear trend analysis, separately for each condition. Results from this analysis were statistically significant only for the location trials [$F_{(1,24)}$ = 5.68, p = 0.025, partial η^2 = .191, Head < Body < Tail], confirming presence of an anterior to posterior gradient in HC activity during spatial learning.

In contrast to encoding, during memory retrieval the HC activity rose gradually as a function of anatomical location along the anterior-posterior axis, regardless of the type of memory being retrieved [linear contrast for Symbols: $F_{(1,24)} = 18.08$, $p < .001$; linear contrast for Locations: $F_{(1,24)} = 36.04$, $p < .001$; linear contrast for Both: $F_{(1,24)} = 7.37$, $p = .012$]. This pattern was driven by BOLD deactivation in the HC head [$t_{(24)} = -4.30$, $p < .001$], and activation in the HC body and tail [body: $t_{(24)} = 3.91$, $p = .001$; tail: $t_{(24)} = 5.45$, $p < .001$] (Fig. 7b, Table 3). Furthermore, direct comparisons of subregions' retrieval activity showed that both posterior subregions were more active than the HC head during retrieval trials [body: $t(24) = 7.85$, $p < 10^{-6}$; tail: $t(24) = 6.12$, $p < 10^{-4}$], while retrieval activities in the body and tail did not differ statistically ($p = .124$). Additionally, encoding vs. retrieval activity differentials were greater in the HC head than in the HC body or tail [head vs. body: $t(24) = 3.69$, $p = .005$; head vs. tail: $t(24) = 3.69$, $p = .026$; body vs. tail, $p = .737$]. Comparing encoding and retrieval activities to each other showed that both anterior (i.e., head) and posterior (body together with tail) segments of the HC formation were more active during the encoding phase than during the retrieval phase [anterior: $t_{(24)} = 6.21$, $p < .001$; posterior: $t_{(24)} = 3.09$, $p = .015$].

fMRI: anterior vs. posterior hippocampal subfields

Finally, we examined the encoding activity in subfields within the anterior (head) and posterior (body together with tail) HC. The posterior HC subfields responded differently during memory encoding [$F_{(2,48)} = 14.16$, $p < .001$, partial $\eta^2 = .371$], which was not the case in the anterior HC ($p = .697$). Furthermore, all subfields within the posterior HC showed different levels of activity [DG vs. CA1-3: $t_{(24)} = 2.63$, $p = 0.030$; DG vs. Sub: $t_{(24)} = 5.65$, $p < .001$; CA1-3 vs. Sub: $t_{(24)} = 2.56$, $p = .017$]. Activities in the anterior and posterior segments of each subfield did not differ

statistically (all ps > .10), implying that underlying activity patterns were similar in both the anterior and posterior HC, although differences in encoding activity were more pronounced in the posterior HC (Fig. 8a, Table 3). Finally, we compared each anterior/posterior subfield's encoding activity (collapsed across hemispheres and conditions) to the baseline task. These tests showed that every subfield in both the anterior and posterior HC was active during the encoding phase (all ps < .050) (see Fig. 8a, Table 3). Consistent with previously described results, we did not observe any activity differences related to trial type (i.e., symbol, location, and both) in any of the anterior or posterior subfields (all ps > .10).

During memory retrieval, all posterior subfields were more active than their anterior counterparts [CA1-3: $t_{(24)}$ = 4.62, p < .001; DG: $t_{(24)}$ = 6.49, p < .001; Sub: $t_{(24)}$ = 3.76, p = .003]. In congruence with the encoding results, all subfields responded similarly in the anterior (p = .222), but not in the posterior HC [$F_{(2,24)}$ = 5.87, p = .010, partial η^2 = .197] (Fig. 8b, Table 3). Within the posterior HC, retrieval-related activity was statistically larger in the DG than in the CA1-3 or Sub [$t_{(24)}$ = 3.82, p = .004; $t_{(24)}$ = 2.72, p = .036, respectively]; however, the CA1-3 retrieval activity did not differ from the Sub activity [$t_{(24)}$ = 0.76, p = .456] (Fig. 8b, Table 3). Examining the posterior HC subfields separately revealed that all subfields were either activated or trended towards activation during memory retrieval [CA1-3: $t_{(24)}$ = 1.95, p = .062; DG: $t_{(24)}$ = 7.55, p < .001; Sub: $t(24)$ = 2.80, p = .020]. This is in contrast to the anterior HC, which, as we described earlier, showed a statistically significant negative BOLD response during memory retrieval (Fig. 8b, Table 3).

Comparing encoding and retrieval activities to each other (Fig. 8c, Table 3) showed that within the anterior HC, every subfield was more active during memory encoding than during memory retrieval [CA1-3: $t_{(24)}$ = 5.49, p < .001; DG: $t_{(24)}$ = 4.82, p < .001; Sub: $t_{(24)}$ = 3.30, p = .009].

Within the posterior HC, encoding vs. retrieval contrasts were significant for the CA1-3 [$t_{(24)}$ = 3.77, p = .004] and DG [$t_{(24)}$ = 2.86, p = .017], but not for the Sub (p = .969). Finally, for every subfield, encoding vs. retrieval activity differences were larger in the anterior HC than in the posterior HC [CA1-3: $t_{(24)}$ = 2.38, p = .050; DG: $t_{(24)}$ = 2.34, p = .028; Sub: $t_{(24)}$ = 2.94, p = .022], and these anterior-posterior differences in encoding vs. retrieval activity were similar in all subfields [p = .668] (Fig. 8c, Table 3).

DISCUSSION

To our knowledge, this is the first fMRI study to examine how anterior-posterior HC subregions and cross-sectional subfields are involved in the encoding and retrieval of item, spatial, and associative memories across the entire HC structure. Four major patterns emerged from our results. First, although all HC subregions and all subfields (in both the anterior and posterior HC) were active during memory encoding, during memory retrieval we observed an anterior-to-posterior gradient in HC activity that was independent of the type of memory being retrieved. This gradient was characterized by above-baseline activity in the posterior HC (HC body and tail) and below-baseline activity in the anterior HC (HC head). Second, we observed larger activity in the DG subfield than in the CA1-3 or Sub during both encoding and retrieval. Third, although our paradigm employed an explicit set of instructions aimed at priming attention to specific aspects of a stimulus, those instructions had minimal effects on HC activity during memory encoding. Fourth, encoding vs. retrieval activity differences were larger in the anterior HC for all subfields, suggesting that the aforementioned anterior-posterior differences in HC function are likely subfield-independent. Finally, to our best knowledge this is the first study to adapt the 'Designs' subtest from the WMS-IV to an fMRI paradigm, and our results provide insight into how the WMS-IV 'Designs' subtest relates to HC function.

28

Previous literature demonstrated that the HC formation plays a crucial role in item-location memory (Allen et al., 2014; Smith & Milner, 1981; Watson et al., 2013). However, whether different types of memory rely on HC to a similar extent is still a matter of scientific debate. There is evidence from fMRI and patient studies showing that memory for relations can be distinguished from memory for spatial information (Eichenbaum, 2017; Eichenbaum & Cohen, 2014; Kumaran & Maguire 2005; Lisman et al., 2017; Nadel et al., 2012), and from memory for items themselves (Caplan & Madan, 2016; Konkel et al., 2008; Madan et al., 2017). Here, we employed an fMRI paradigm, based on the 'Designs' subtest from the WMS-IV, to perform direct comparisons of HC activity during encoding and retrieval of item, spatial, and associative memories.

Despite the widespread clinical use of the WMS-IV, little research has been done on the 'Designs' subtest (Martin & Schroeder, 2014), and especially on how it relates to brain function. Studies have shown that this task assesses visual attention and visual memory, and shares common factor loadings with tests of visual reproduction (Hoelzle et al., 2011; Holdnack et al., 2011). The 'Designs' subtest itself is a modification of the 'Memory for Designs' subtest found in the Developmental Neuropsychological Assessment, second edition (NEPSY-II), a neuropsychological battery commonly used in pediatric studies (Brooks et al., 2009, 2010). Those studies have shown that performance on 'Memory for Designs' shares little variance with other NEPSY-II tests of visual memory, such as 'Memory for Faces' and 'Memory for Names' (Brooks et al., 2010), suggesting that at least in children this task relies on a different set of cognitive processes than face recognition or formation of visual-auditory associations.

Although this is the first fMRI adaptation of the 'Designs' subtest, our paradigm has much in common with item-location memory tasks (Horecka et al. 2018; Kessels et al. 2002; Owen et al.,

1996; Postma et al., 2008; Smith & Milner, 1981), except for one major difference: we used abstract images instead of pictures of everyday objects or faces. In general, abstract images are more suitable for studying item memory because participants are less able to use pre-existing semantic knowledge and associations to support the task-specific episodic memory, and thus, contaminate the test of item memory itself. Other researchers (e.g., Konkel et al., 2008) have also used highly abstract novel objects in their tests of item and relational memory for very similar reasons.

Despite the fact that most fMRI studies focused on one type of information at a time, several fMRI and neuropsychological studies attempted to compare the HC role in processing of spatial vs. non-spatial memories (Horecka et al., 2018; Konkel et al., 2008; Kumaran & Maguire, 2005; Ryan et al., 2010). For example, Kumaran and Maguire (2005) reported that BOLD activity in the HC formation was correlated with spatial-relational, but not social-relational memory. The authors also reported that neither the spatial nor the relational processing alone was sufficient to activate the HC, but that the combination of the two factors was crucial for the HC engagement. Another research group (Ryan et al., 2010) used a within-subject design to separate spatial and non-spatial relations from episodic and semantic memory during memory retrieval. In agreement with the cognitive map theory (O'Keefe & Nadel, 1978), spatial relations (collapsed across episodic-spatial, semantic-spatial-old and semantic-spatial-new) engaged the HC to a greater degree than non-spatial relations, while no voxels showed the opposite pattern (nonspatial > spatial). In contrast, a study by Konkel and colleagues (2008) demonstrated that amnesic patients, with HC-specific damage, were impaired not only on all tests of relational memory, including spatial, associative, and sequential, but also on tests of item memory, although performance on the former was more affected than performance on the latter (Konkel et al.,

2008). Our results also suggest domain-agnostic nature of HC function, especially during memory encoding.

Even though we did not detect any condition-related differences within any of our HC ROIs, we observed global laterality effects for retrieval of spatial memories. These results are in agreement with studies of MTL patients, which showed that memories for spatial relationships are particularly susceptible to right, but not left, HC damage (Kessels et al., 2002; van Asselen et al., 2008). Our work builds on those previous findings by demonstrating that left vs. right HC differences were present in all HC subfields, in both the anterior and posterior HC segments. However, our results showed that these hemispheric effects were present only during the retrieval phase, and only for spatial memory. This further extends our knowledge of encoding/retrieval differences in HC function, particularly as they related to spatial tasks.

In addition to comparing different memory components, our design enabled us to examine both longitudinal and cross-sectional properties of the HC architecture. Anatomical connectivity studies showed that splitting the HC into just two (i.e., anterior and posterior sections) sections might lead to oversimplified models of its function (Small et al., 2002; Strange et al. 2014). Such anterior/posterior subdivisions often do not correspond to anatomical properties of the HC; instead, the HC (or the entire MTL) is split into two or three long-axis segments of approximately equal length (Ranganath & Ritchey, 2012; Small et al., 2002). In contrast, when the HC was subdivided in accordance with anatomical properties, all three subregions (i.e., head, body, and tail) showed different patterns of connectivity (Ranganath & Ritchey, 2012), different subfield compositions (Malykhin et al., 2010, 2017), and unique roles in episodic memory (Chen et al., 2010; DeMaster et al., 2014; Evensmoen et al., 2013; Spalletta et al., 2016; Travis et al, 2014; de Vanssay-Maigne et al. 2011). Our results showed that the level of activity in the HC

body was somewhere between that of the head and that of the tail, suggesting that anterior-posterior differences might be organized along a gradient rather than being a simple dichotomy. These observations are consistent with a recent meta-analysis by Kim (2015) as well as theoretical framework outlined by Poppenk and colleagues (2013): both emphasize that the anterior versus posterior functional specialization is a relative difference, not a sharp dichotomy.

It has been suggested that the anterior and posterior HC are specialized for encoding and retrieval, respectively (Kim, 2015; Lepage et al., 1998; Schacter & Wagner, 1999; Spaniol et al., 2009); however, experiments by Greicius et al. (2003) and Schacter et al. (1999) reported encoding-related activity in both anterior and posterior segments of the HC formation. One major limitation of most standard-resolution studies of HC function is the high degree of smoothness among activation clusters, which in the anterior HC can bleed into the amygdala nuclei, and in the posterior HC tend to overlap with the nearby MTL cortices. Since we did not smooth our data and used manual segmentation to define each anterior-posterior subregion in native space, we were able to isolate the HC formation from surrounding MTL structures. Our results agree with both of the aforementioned arguments because (1) all 3 HC subregions were active (relative to odd/even baseline) during memory encoding, and (2) the encoding vs. retrieval activity differential was larger in the HC head than in the HC body or tail. However, it remains to be determined whether HC subregions perform similar functions in memory encoding or whether they encode different aspects of a stimulus. The latter view is partially supported by our results from spatial trials, for which we observed an anterior to posterior gradient in BOLD activation. Similar anteroposterior differentials in HC activity for spatial memory have been reported in primates (Colombo et al., 1998), while human imaging studies reported (1) greater activity in the right posterior HC during tasks with a spatial memory component (Banks et al., 2012;

Hoscheidt et al., 2010; Ryan et al., 2010), and (2) enlargement of the posterior HC in London taxi drivers with expert knowledge of the city (Maguire et al., 2000, 2003; Woollett et al., 2009; Woollett and Maguire, 2011). Interestingly, London taxi drivers eventually experience a loss of gray matter volume in the anterior HC, and as years on the road increase, become less proficient on memory tasks requiring formation of novel object-location associations (Woollett & Maguire, 2009, 2012). Presumably this is a consequence of heavy reliance on memory retrieval processes during daily work-related activities. As demonstrated by our results, retrieval of all types of memories engages the posterior HC, while metabolic demands on the HC head during memory retrieval were less than those required to perform the baseline odd/even judgment task.

In recent years interest has shifted towards the function of the HC subfields in episodic memory (e.g., Azab et al., 2014; Bakker et al., 2008; Chen et al., 2011; Copara et al., 2014; Das et al., 2011; Eldridge et al., 2005; Preston et al., 2010; Reagh et al., 2014; Suthana et al., 2011, 2015; Yassa et al., 2011; Zeineh et al., 2003) with much of this work aimed at elucidating neural correlates of pattern separation and pattern completion processes (Bakker et al., 2008; Duncan et al., 2012; Lacy et al., 2011; Yassa and Stark, 2011). Both animal and computational literature (Hasselmo et al., 1995; Lisman & Grace, 2005; Meeter et al., 2004; Norman and O'Reilly, 2003; Vinogradova, 2001) suggest that the HC is a dynamic system, continuously shifting between integration and discriminations states in response to task demands. Recent high-resolution fMRI (Azab et al., 2014; Bakker et al., 2008; Berron et al., 2016; Duncan et al., 2012; Lacy et al., 2011) and patient work (Baker et al., 2016) confirmed the DG (or DG/CA3), role in pattern separation. However, unlike our task, most pattern separation/completion studies employed incidental (as opposed to explicit) encoding paradigms and studied HC processes responsible for laying down separate memory traces from similar perceptual inputs. Interestingly, these studies

indicate that the DG/CA3 subfield acts as universal pattern separator (Azab et al., 2014; Bakker et al., 2008; Copara et al., 2014; Lacy et al., 2011), meaning that its basic role of laying down distinct memory traces from overlapping information is similar for item, spatial, and temporal information. Although our task did not employ incidental learning and was not designed to study integration/discrimination states, we also observed similar degree of activation for all types of learning in every subfield.

In addition to pattern separation/completion studies, the DG/CA3 subfield demonstrated involvement in memory tasks with a spatial component: it showed robust activity to specific spatial cues in overlapping navigational environments (Brown et al., 2014), sensitivity to changes in spatial–contextual input (Stokes et al., 2015), and was activated during retrieval of both spatial and temporal information (Copara et al., 2014). In contrast, Zeidman and Maguire (2016) implicated the anterior presubiculum and parasubiculum in tasks involving the construction and recall of scenes. However, Kyle and colleagues (2015) found that retrieving information regarding spatial or temporal proximity of elements within spatial or temporal context resulted in similar patterns of activity spanning multiple HC subfields.

From previous research on explicit associative memory a general pattern of subfield specialization emerges: preferential role of the DG/CA23 in encoding processes and subiculum in retrieval processes (Eldridge et al., 2005; Suthana et al., 2015; Zeineh et al., 2003). A similar pattern was also reported in a task employing spatial learning using navigation-like video clips (Suthana et al., 2011). However, no direct comparisons of HC subfield activity during different types of learning were carried out since paradigms studying spatial and associative memories were acquired on different subjects, using different baseline tasks, and sometimes even different MRI systems. Furthermore, because of technical limitations some of those studies did not

segment the most anterior and the most posterior segments of the HC structure (e.g., Chen et al., 2011; Eldridge et al., 2005; Suthana et al., 2011; Zeineh et al., 2003). Our results filled the gap in this literature by: (1) showing that all three subfields were active during memory encoding, regardless of which memory domain was involved, and (2) further demonstrating that task-related signal changes in the CA1-3 and Sub were half the magnitude of those in the DG. Even during the retrieval phase, our results implicate greater involvement of the DG, as opposed to the CA1-3 or Sub. In contrast to the results reported by Eldridge et al. (2005), Suthana et al. (2015), and Zeineh et al. (2003), we did not observe total Sub activation during memory retrieval. Differences among studies of Sub function can be partially attributed to differences in subfield segmentation protocols used by different research groups (Malykhin et al., 2017; Yushkevich et al., 2015a). Studies, which reported increased Sub activity during memory retrieval, generally included the presubiculum and parasubiculum within their Sub ROIs, while our segmentation protocol was designed to isolate the Sub proper. Consequently, it is plausible that presubiculum and parasubiculum are more active than the Sub proper during memory retrieval. Lastly, our results showed that the encoding vs. retrieval activity differences were larger in the anterior HC in every subfield, suggesting that the aforementioned anterior-posterior differences in HC function are subfield-independent. Further work is needed to explain why this is the case.

At the cellular level, encoding/retrieval differences in subfield function could be driven by their connectivity profiles. During encoding, most models emphasize sequential steps of information processing within the trisynaptic circuit: from entorhinal cortex (EC) to the DG, then via CA3 to CA1, with final outputs to Sub, EC and parahippocampal regions (Jones & McHugh, 2011). However, new memories can also be rapidly encoded in CA1 through direct projections from the EC to the CA1, and CA2 subfields (Jones & McHugh, 2011). In contrast, during memory

retrieval information does not flow directly from the EC to the CA1-2, and instead passes through the DG or CA3 subfields first (Jones & McHugh, 2011). This emphasizes the importance of the DG and CA3 for both encoding and retrieval of episodic memories, whilst the inputs to CA1-2 vary between those two states. Despite the fact that both the CA1 and Sub serve as the major output regions of the HC (O'Mara, 2006), Sub involvement in encoding processes is less clear.

To our best knowledge there is only one study to date (Reagh et al., 2014), which clearly demonstrated subfield-specific long-axis differences in HC function in relationship to memory. In that study the anterior (mostly head) DG/CA3 region displayed repetition suppression effects, while the posterior (mostly body and tail) DG/CA3 showed activity enhancement for previously studied highly familiar scenes, such as Mona Lisa, Eiffel Tower, and Taj Mahal. Although no explicit memory tests were carried out, it is plausible that neural correlates of individual stimuli were reinstated in the posterior DG/CA3. Recent work by Tompary and colleagues (2016) suggests that successful memory retrieval is driven by the reinstatement of encoding-related activity within the CA1 subfield, although CA23DG region showed a similar trend. Whether anterior or posterior segments of the HC subfields are the main drivers of pattern reinstatement is largely unknown. Based on our results, we think that the posterior DG is particularly important for memory reinstatement, although we were not able to test this hypothesis directly due to the insufficient number of forgotten trials. Together with work done by Reagh et al. (2014), our results demonstrate the importance of considering both the anterior-posterior and the transverse axis properties of HC architecture, when carrying out studies of HC function. In light of recent evidence that the anterior, but not posterior, Sub plays an important role in basic scene

discrimination (Hodgetts et al., 2017), it is advisable to account for the longitudinal differences in subfield function even in tasks other than memory.

In addition to providing insight into how the HC anatomy relates to memory processes, our analysis methodology suggests that retrieval- and encoding-related changes in neural firing within the HC occur on a sub-TR scale. As seen in Figure 4, encoding-related BOLD in the HC peaked 4-5 seconds after trial onset (on average), and retrieval-related BOLD response peaked 6-7 seconds after the trial onset, indicating relatively short-lasting changes in HC activity evoked by memory processes. This further highlights the importance of estimating hemodynamic response in each brain region individually, separately for each task. Assuming constant increase/decrease in neural firing rate for the entire trial duration (e.g., for 10 s during encoding in our design) is likely to result in inaccurate assumptions about neural and vascular properties in different brain regions. Recent work by Nauer and colleagues (2015) pointed out similar pitfalls in assuming sustained HC firing, which produced surprisingly poor models of the HC BOLD response.

Limitations and future directions

Except for hemispheric differences during the retrieval phase, we did not find any statistical differences between item, spatial, and associative memories. Consistent with our observations, a number of other studies, comparing different memory domains also reported a lack of difference in HC activity (Azab et al., 2014; Ekstrom et al., 2011) and similar subfield activity patterns were reported in a variety of memory tasks (Suthana et al., 2009, 2011; Eldridge et al., 2005; Zeineh et al., 2003). However, it should be noted that whenever a study with a modest sample size fails to find statistical differences, the issue of statistical power comes to mind (Button et al.,

2013). Although our study employed a larger sample size than many recent fMRI studies of the HC subfields (e.g., Aly & Turk-Browne, 2016; Azab et al., 2014; Copara et al., 2012; Duncan et al., 2014; Reagh et al., 2014; Suthana et al., 2015; Stokes et al., 2015; Tompary et al., 2016; all with sample sizes in the range of 14-22 participants), it is plausible that a larger number of trials per condition and/or a larger number of subjects is required to detect relatively subtle differences in subfield activity, particularly when comparing HC activity during encoding/retrieval of different types of memory. Alternatively, multivoxel classification techniques might be able to detect differences in patterns of activity within subfields for different types of memory. However, this also requires a greater number of trials than were feasible in the current study. Furthermore, our study sample consisted primarily of younger adults (mostly undergraduate and graduate students, 20-33 years of age) and future studies will need to investigate the extent to which our findings are relevant to individuals from different populations. For instance, in our recent aging study (Malykhin et al., 2017) we demonstrated that subfields within the HC body are particularly vulnerable to age-related atrophy, while subfields within the HC head and tail showed minor, if any, age-related effects. It is currently unclear whether those structural changes contribute to changes in BOLD activity within various HC subregions and subfields and if so, whether those functional changes can explain age effects on performance in visuospatial memory tasks.

On the technical side, some limitations related to our data and segmentation protocol must be pointed out. Although there were no differences in head motion between symbol, location, and both trial types, our participants were more likely to move during memory encoding than during memory retrieval, regardless of memory condition. During the encoding phase, on average 1.8 out of 12 trials per condition were affected, while 1.1 out of 12 trials per condition were affected

during the retrieval phase. However, considering strict scrubbing thresholds and extensive denoising procedures that we employed during our preprocessing, it is unlikely that these differences in head motion played a consequential role in our encoding vs. retrieval tests.

Furthermore, because of methodological constraints, we were unable to study activity in the individual CA subfields. According to post-mortem work (Adler et al., 2014; Rössler et al., 2002; Simić et al., 1997), the CA23 segment takes up 6-10% of the total HC volume. Recent attempts at segmenting the CA1, CA2, and CA3 structural MRI reported similar proportions (Goubran et al., 2013; Iglesias et al., 2015; Winterburn et al., 2013; Wisse et al., 2012; Yushkevich et al., 2015b), and a recent 7 T study by Suthana and colleagues (2015) attempted to compare encoding and retrieval activities in each individual CA subfield. Those results showed that the CA3 subfield is particularly important for memory encoding. Given spatial resolution limitations of our fMRI data (1.5-mm isotropic voxels), the combined CA23 volume is expected to consist of two to three voxels on each coronal slice of the HC body, with the CA3 and CA2 subfields being one voxel large on most slices. Because of the inherent spatial blur in all fMRI datasets (approximately 2 mm FWHM within the HC formation for our fMRI images), partial volume effects, geometric distortions caused by B_0 inhomogeneity, and imperfections in motion correction by realignment techniques, the anatomical validity of one- or two-voxel activity localization would be tenuous at best. Furthermore, since the DG/CA3, CA3/CA2, and CA2/CA1, and CA1/Sub tissue boundaries are not visible on *in vivo* ultra-high-resolution T2-weighted structural MRI even at 7 T (Berron et al., 2016; Suthana et al., 2015; Yushkevich et al., 2015a), there are substantial disagreements between various research groups as to where those boundaries ought to be placed (see Yushkevich et al., 2015a for protocol comparisons). For instance, our CA1/Sub boundary is more lateral than that of some other

studies of subfield function (Bonnici et al., 2012; Copara et al., 2014; Eldridge et al., 2005; Stokes et al., 2015; Suthana et al., 2009, 2011, 2015; Zeineh et al., 2003). Furthermore, some studies included the presubiculum and parasubiculum within their Sub ROIs (e.g., Copara et al., 2014; Eldridge et al., 2005; Stokes et al., 2015; Suthana et al., 2009, 2011, 2015; Zeineh et al., 2003), while others (e.g., Bakker et al., 2008; Bonnici et al., 2012; Lacy et al., 2011; Tompary et al. 2016), including this study, excluded most of the presubiculum and parasubiculum from their Sub ROIs. As a result, it is best to exercise caution when relating results from various laboratories studying HC subfield function since subfield ROIs, despite similar naming, might in fact represent different HC anatomy (Yushkevich et al., 2015a). Across 21 subfield segmentation protocols employed by various research groups, only the DG/CA4 region within the HC body showed a high degree of agreement. Fortunately, this is a well-known issue in the field and efforts at developing a harmonized subfield segmentation protocol are underway (Yushkevich et al., 2015a).

In the present study, we employed a manual classification procedure during our HRf model-building step. Manual classification and de-noising of fMRI signals following independent component analysis (ICA) decompositions is well-documented (Griffanti et al., 2017; Salimi-Khorshidi et al., 2014), and although a number of automated component classifiers have been developed, visual inspection of each ICA component by an expert rater is still the gold standard in the field against which automated techniques are evaluated (Bhaganagarapu et al., 2013, Perlbarg et al., 2007, Rummel et al., 2013, Salimi-Khorshidi et al., 2014; Storti et al., 2013; Tohka et al., 2008). Similarly, future studies might benefit from developing a fully automated procedure for classifying estimated HRfs as activation, deactivation, or noise based on previously established criteria by expert raters. However, such development and validation of

automated HRf classification procedures was not within the primary scope of the current work. Similar to ICA-based techniques, any future automated HRf classification would need to be validated/tested against manual classification prior to being applied in fMRI research.

Lastly, although the HC is crucial to memory processes, it is not the only brain structure needed for memory formation, maintenance, and retrieval. An extensive body of literature implicates the entorhinal, perirhinal, and parahippocampal cortices in memory (Kensinger, 2009; Moscovitch et al., 2016; Roy et al., 2017; Squire & Dede, 2015; Small, 2002; Spaniol et al., 2009; Tompary et al., 2016). Consequently, further work is needed to investigate the role that other brain regions perform in 'Designs'-like tests of visuospatial memory. Furthermore, even though our current study focused on memory formation and retrieval, the HC performs important functions in stress response, contextual fear conditioning, decision making, imagination, and even perceptual discrimination (Bannerman et al., 2003, 2004, 2014; Lee et al., 2005; Murray et al., 2007; O'Neil et al., 2015; Pentkowski et al., 2006; Suzuki & Baxter, 2009; Zeidman & Maguire, 2016). How the HC subfields within particular longitudinal segments relate to cognitive processes other than episodic memory is largely unexplored (but see, Hodgetts et al., 2017; Leal et al., 2017; Zeidman et al., 2015 for recent attempts).

CONCLUSION

We used anatomical landmarks to extract BOLD activities from the HC transverse subfields and longitudinal subregions, and examined their role in memory encoding and memory retrieval. Our results showed that all subfields in the anterior and posterior segments of the HC formation were active during the encoding phase, whilst during memory retrieval we observed an anterior to posterior gradient in HC activity. Our findings also confirmed presence of an anterior to

posterior gradient in HC activity during spatial learning. The DG was more active than the CA1-3 or Sub during both encoding and recall. Furthermore, our results suggest that metabolic demands on the HC subfields and subregions are similar for item, spatial, and relational memories, especially during the encoding phase. Lastly, our results provide insight into how the WMS-IV 'Designs' subtest relates to HC function. Future high-field high-resolution fMRI studies of episodic memory will allow researchers to further understand the structure–function relationship of the human HC and its complex anatomy.

REFERENCES

Adler, D. H., Pluta, J., Kadivar, S., Craige, C., Gee, J. C., Avants, B. B., & Yushkevich, P. A. (2014). Histology-derived volumetric annotation of the human hippocampal subfields in postmortem MRI. *NeuroImage*, *84*, 505–523.

Allen, R. J., Vargha-Khadem, F., & Baddeley, A. D. (2014). Item-location binding in working memory: is it hippocampus-dependent? *Neuropsychologia*, *59*, 74–84.

Aly, M., & Turk-Browne, N. B. (2016). Attention Stabilizes Representations in the Human Hippocampus. *Cerebral Cortex*, *26*(2), 783–796.

Andersson, J. L., Hutton, C., Ashburner, J., Turner, R., & Friston, K. (2001). Modeling geometric deformations in EPI time series. *NeuroImage*, *13*(5), 903–919.

Azab, M., Stark, S. M., & Stark, C. E. L. (2014). Contributions of human hippocampal subfields to spatial and temporal pattern separation. *Hippocampus*, *24*(3), 293–302.

Baker, S., Vieweg, P., Gao, F., Gilboa, A., Wolbers, T., Black, S. E., & Rosenbaum, R. S. (2016). The human dentate gyrus plays a necessary role in discriminating new memories. *Current Biology*, *26*(19), 2629–2634.

Bakker, A., Kirwan, C. B., Miller, M., & Stark, C. E. (2008). Pattern separation in the human hippocampal CA3 and dentate gyrus. *Science*, *319*(5870), 1640–1642.

Bannerman, D. M., Grubb, M., Deacon, R. M. J., Yee, B. K., Feldon, J., & Rawlins, J. N. P. (2003). Ventral hippocampal lesions affect anxiety but not spatial learning. *Behavioural Brain Research*, *139*(1-2), 197–213.

Bannerman, D. M., Rawlins, J. N. P., McHugh, S. B., Deacon, R. M. J., Yee, B. K., Bast, T., Zhang, W. N., Pothuize, H. H., & Feldon, J. (2004). Regional dissociations within the hippocampus–memory and anxiety. *Neuroscience and Biobehavioral Reviews*, *28*(3), 273–283.

Bannerman, D. M., Sprengel, R., Sanderson, D. J., McHugh, S. B., Rawlins, J. N. P., Monyer, H., & Seeburg, P. H. (2014). Hippocampal synaptic plasticity, spatial memory and anxiety. *Nature Reviews. Neuroscience*, *15*(3), 181–192.

Banks, S. J., Sziklas, V., Sodums, D. J., & Jones-Gotman, M. (2012). fMRI of verbal and nonverbal memory processes in healthy and epileptogenic medial temporal lobes. *Epilepsy & Behavior*, *25*(1), 42–49.

Berron, D., Schütze, H., Maass, A., Cardenas-Blanco, A., Kuijf, H. J., Kumaran, D., & Düzel, E. (2016). Strong Evidence for Pattern Separation in Human Dentate Gyrus. *Journal of Neuroscience*, *36*(29), 7569–7579.

Bhaganagarapu, K., Jackson, G. D., & Abbott, D. F. (2013). An automated method for identifying artifact in independent component analysis of resting-state fMRI. *Frontiers in Human Neuroscience*, *7*.

Birn, R. M., Diamond, J. B., Smith, M. A., & Bandettini, P. A. (2006). Separating respiratory-variation-related fluctuations from neuronal-activity-related fluctuations in fMRI. *NeuroImage*, *31*(4), 1536–1548.

Birn, R. M., Smith, M. A., Jones, T. B., & Bandettini, P. A. (2008). The respiration response function: the temporal dynamics of fMRI signal fluctuations related to changes in respiration. *NeuroImage*, *40*(2), 644–654.

Boccardi, M., Bocchetta, M., Ganzola, R., Robitaille, N., Redolfi, A., Duchesne, S., Jack, C. R., & Frisoni, G. B. (2015). Operationalizing protocol differences for EADC-ADNI manual hippocampal segmentation. *Alzheimer's & Dementia*, *11*(2), 184–194.

Bonne, O., Vythilingam, M., Inagaki, M., Wood, S., Neumeister, A., Nugent, A. C., Snow, J., Luckenbaugh, D. A., Bain, E. E., Drevets, W. C., & Charney, D. S. (2008). Reduced posterior hippocampal volume in posttraumatic stress disorder. *Journal of Clinical Psychiatry*, *69*(7), 1087–1091.

Bonnici, H. M., Chadwick, M. J., Kumaran, D., Hassabis, D., Weiskopf, N., & Maguire, E. A. (2012). Multi-voxel pattern analysis in human hippocampal subfields. *Frontiers in Human Neuroscience*, *6*, 290.

Bouchard, T. P., Malykhin, N., Martin, W. R. W., Hanstock, C. C., Emery, D. J., Fisher, N. J., & Camicioli, R. M. (2008). Age and dementia-associated atrophy predominates in the hippocampal head and amygdala in Parkinson's disease. *Neurobiology of Aging*, *29*(7), 1027–1039.

Brooks, B. L., Sherman, E. M. S., & Strauss, E. (2010). Test Review: NEPSY-II: A developmental neuropsychological assessment, Second edition. *Child Neuropsychology, 16*(1), 80-101.

Brooks, B. L., Strauss, E., Sherman, E. M. S., Iverson, G. L., & Slick, D. J. (2009). Developments in neuropsychological assessment: Refining psychometric and clinical interpretive methods. *Canadian Psychology*, *50*(3), 196–209.

Brown, T. A., Di Nardo, P. A., Lehman, C. L., & Campbell, L. A. (2001). Reliability of DSM-IV anxiety and mood disorders: implications for the classification of emotional disorders. *Journal of Abnormal Psychology*, *110*(1), 49–58.

Brown, T. I., Hasselmo, M. E., & Stern, C. E. (2014). A high-resolution study of hippocampal and medial temporal lobe correlates of spatial context and prospective overlapping route memory. *Hippocampus*, *24*(7), 819–839.

Button, K. S., Ioannidis, J. P. A., Mokrysz, C., Nosek, B. A., Flint, J., Robinson, E. S. J., & Munafò, M. R. (2013). Power failure: why small sample size undermines the reliability of neuroscience. *Nature Reviews. Neuroscience*, *14*(5), 365–376.

Calhoun, V. D., Stevens, M. C., Pearlson, G. D., & Kiehl, K. A. (2004). fMRI analysis with the general linear model: removal of latency-induced amplitude bias by incorporation of hemodynamic derivative terms. *NeuroImage*, *22*(1), 252–257.

Caplan, J. B., & Madan, C. R. (2016). Word Imageability Enhances Association-memory by Increasing Hippocampal Engagement. *Journal of Cognitive Neuroscience*, *28*(10), 1522–1538.

Chang, C., Cunningham, J. P., & Glover, G. H. (2009). Influence of heart rate on the BOLD signal: the cardiac response function. *NeuroImage*, *44*(3), 857–869.

Chen, K. H. M., Chuah, L. Y. M., Sim, S. K. Y., & Chee, M. W. L. (2010). Hippocampal region-specific contributions to memory performance in normal elderly. *Brain and Cognition*, *72*(3), 400–407.

Chen, J., Olsen, R. K., Preston, A. R., Glover, G. H., & Wagner, A. D. (2011). Associative retrieval processes in the human medial temporal lobe: hippocampal retrieval success and CA1 mismatch detection. *Learning & Memory*, *18*(8), 523–528.

Chua, E. F., Schacter, D. L., Rand-Giovannetti, E., & Sperling, R. A. (2007). Evidence for a specific role of the anterior hippocampal region in successful associative encoding. *Hippocampus*, *17*(11), 1071–1080.

Cohen, N. J., & Eichenbaum, H. (1993). Memory, amnesia, and the hippocampal system. Cambridge, MA, US: The MIT Press.

Cohen, N. J., Ryan, J., Hunt, C., Romine, L., Wszalek, T., & Nash, C. (1999). Hippocampal system and declarative (relational) memory: summarizing the data from functional neuroimaging studies. *Hippocampus*, *9*(1), 83–98.

Colombo, M., Fernandez, T., Nakamura, K., & Gross, C. G. (1998). Functional differentiation along the anterior-posterior axis of the hippocampus in monkeys. *Journal of Neurophysiology*, *80*(2), 1002–1005.

Copara, M. S., Hassan, A. S., Kyle, C. T., Libby, L. A., Ranganath, C., & Ekstrom, A. D. (2014). Complementary roles of human hippocampal subregions during retrieval of spatiotemporal context. *Journal of Neuroscience*, *34*(20), 6834–6842.

Das, S. R., Mechanic-Hamilton, D., Pluta, J., Korczykowski, M., Detre, J. A., & Yushkevich, P. A. (2011). Heterogeneity of functional activation during memory encoding across hippocampal subfields in temporal lobe epilepsy. *NeuroImage*, *58*(4), 1121–1130.

Daugherty, A. M., Yu, Q., Flinn, R., & Ofen, N. (2015). A reliable and valid method for manual demarcation of hippocampal head, body, and tail. *International Journal of Developmental Neuroscience*, *41*, 115–122.

Davachi, L., Mitchell, J. P., & Wagner, A. D. (2003). Multiple routes to memory: distinct medial temporal lobe processes build item and source memories. *Proceedings of the National Academy of Sciences of the United States of America*, *100*(4), 2157–2162.

DeMaster, D., Pathman, T., Lee, J. K., & Ghetti, S. (2014). Structural development of the hippocampus and episodic memory: developmental differences along the anterior/posterior axis. *Cerebral Cortex*, *24*(11), 3036–3045.

Devonshire, I. M., Papadakis, N. G., Port, M., Berwick, J., Kennerley, A. J., Mayhew, J. E. W., & Overton, P. G. (2012). Neurovascular coupling is brain region-dependent. *NeuroImage*, *59*(3), 1997–2006.

Ding, S.-L., & Van Hoesen, G. W. (2015). Organization and detailed parcellation of human hippocampal head and body regions based on a combined analysis of cyto- and chemoarchitecture. *Journal of Comparative Neurology*, *523*(15), 2233–2253.

Dolcos, F., LaBar, K. S., & Cabeza, R. (2004). Interaction between the amygdala and the medial temporal lobe memory system predicts better memory for emotional events. *Neuron*, *42*(5), 855–863.

Duncan, K., Ketz, N., Inati, S. J., & Davachi, L. (2012). Evidence for area CA1 as a match/mismatch detector: a high-resolution fMRI study of the human hippocampus. *Hippocampus*, *22*(3), 389–398.

Duvernoy, H. M. (2005). *The human hippocampus: Functional anatomy, vascularization, and serial sections with MRI, third ed.* Springer-Verlag. Berlin; New York, p. 232.

Eichenbaum, H. (2001). The hippocampus and declarative memory: cognitive mechanisms and neural codes. *Behavioural Brain Research*, *127*(1–2), 199–207.

Eichenbaum, H. (2017). On the Integration of Space, Time, and Memory. *Neuron*, *95*(5), 1007–1018.

Eichenbaum, H., & Cohen, N. J. (2014). Can we reconcile the declarative memory and spatial navigation views on hippocampal function? *Neuron*, *83*(4), 764–770.

Ekstrom, A. (2010). How and when the fMRI BOLD signal relates to underlying neural activity: the danger in dissociation. *Brain Research Reviews*, *62*(2), 233–244.

Ekstrom, A. D., Copara, M. S., Isham, E. A., Wang, W.-C., & Yonelinas, A. P. (2011). Dissociable networks involved in spatial and temporal order source retrieval. *NeuroImage*, *56*(3), 1803–1813.

Eldridge, L. L., Engel, S. A., Zeineh, M. M., Bookheimer, S. Y., & Knowlton, B. J. (2005). A dissociation of encoding and retrieval processes in the human hippocampus. *Journal of Neuroscience*, *25*(13), 3280–3286.

Elliott, C. A., Gross, D. W., Wheatley, B. M., Beaulieu, C., & Sankar, T. (2016). Progressive contralateral hippocampal atrophy following surgery for medically refractory temporal lobe epilepsy. *Epilepsy Research*, *125*, 62–71.

Evensmoen, H. R., Lehn, H., Xu, J., Witter, M. P., Nadel, L., & Håberg, A. K. (2013). The anterior hippocampus supports a coarse, global environmental representation and the posterior hippocampus supports fine-grained, local environmental representations. *Journal of Cognitive Neuroscience*, *25*(11), 1908–1925.

Frisoni, G. B., Ganzola, R., Canu, E., Rüb, U., Pizzini, F. B., Alessandrini, F., Zoccatelli, G., Beltramello, A., Caltagirone, C., & Thompson, P. M. (2008). Mapping local hippocampal changes in Alzheimer's disease and normal ageing with MRI at 3 Tesla. *Brain*, *131*(Pt 12), 3266–3276.

Glover, G. H. (1999). Deconvolution of impulse response in event-related BOLD fMRI. *NeuroImage*, *9*(4), 416–429.

Glover, G. H., Li, T. Q., & Ress, D. (2000). Image-based method for retrospective correction of physiological motion effects in fMRI: RETROICOR. *Magnetic Resonance in Medicine*, *44*(1), 162–167.

Gold, J. J., Smith, C. N., Bayley, P. J., Shrager, Y., Brewer, J. B., Stark, C. E. L., Hopkins, R. O., & Squire, L. R. (2006). Item memory, source memory, and the medial temporal lobe: concordant findings from fMRI and memory-impaired patients. *Proceedings of the National Academy of Sciences of the United States of America*, *103*(24), 9351–9356.

Goubran, M., Rudko, D. A., Santyr, B., Gati, J., Szekeres, T., Peters, T. M., & Khan, A. R. (2013). In vivo normative atlas of the hippocampal subfields using multi-echo susceptibility imaging at 7 Tesla. *Human Brain Mapping*, *35*(8), 3588–3601.

Goutte C., Nielsen F. A., & Hansen L. K. (2000). Modeling the haemodynamic response in fMRI using smooth FIR filters. *IEEE Transactions on Medical Imaging*, *19*, 1188–1201.

Greicius, M. D., Krasnow, B., Boyett-Anderson, J. M., Eliez, S., Schatzberg, A. F., Reiss, A. L., & Menon, V. (2003). Regional analysis of hippocampal activation during memory encoding and retrieval: fMRI study. *Hippocampus*, *13*(1), 164–174.

Griffanti, L., Douaud, G., Bijsterbosch, J., Evangelisti, S., Alfaro-Almagro, F., Glasser, M. F., et al. (2017). Hand classification of fMRI ICA noise components. *NeuroImage*, *154*, 188–205.

Griswold, M.A., Jakob, P.M., Heidemann, R.M., Nittka, M., Jellus, V., Wang, J., Kiefer, B., Haase, A. (2002). Generalized autocalibrating partially parallel acquisitions (GRAPPA). *Magnetic Resonance in Medicine*, *47*(6), 1202–1210.

Handwerker, D. A., Ollinger, J. M., & D'Esposito, M. (2004). Variation of BOLD hemodynamic responses across subjects and brain regions and their effects on statistical analyses. *NeuroImage*, *21*(4), 1639–1651.

Hasselmo, M. E., Schnell, E., & Barkai, E. (1995). Dynamics of learning and recall at excitatory recurrent synapses and cholinergic modulation in rat hippocampal region CA3. *Journal of Neuroscience*, *15*(7 Pt 2), 5249–5262.

Hayes, J. P., LaBar, K. S., McCarthy, G., Selgrade, E., Nasser, J., Dolcos, F., VISN 6 Mid-Atlantic MIRECC workgroup, & Morey, R. A. (2011). Reduced hippocampal and amygdala activity predicts memory distortions for trauma reminders in combat-related PTSD. *Journal of Psychiatric Research*, *45*(5), 660–669.

Henson, R. N. A., Price, C. J., Rugg, M. D., Turner, R., & Friston, K. J. (2002). Detecting latency differences in event-related BOLD responses: application to words versus nonwords and initial versus repeated face presentations. *NeuroImage*, *15*(1), 83–97.

Hodgetts, C. J., Voets, N. L., Thomas, A. G., Clare, S., Lawrence, A. D., & Graham, K. S. (2017). Ultra-high-field fMRI reveals a role for the subiculum in scene perceptual discrimination. *Journal of Neuroscience*, *37*(12), 3150–3159.

Hoelzle, J. B., Nelson, N. W., & Smith, C. A. (2011). Comparison of Wechsler Memory Scale-Fourth Edition (WMS-IV) and Third Edition (WMS-III) dimensional structures: improved ability to evaluate auditory and visual constructs. *Journal of Clinical and Experimental Neuropsychology*, *33*(3), 283–291.

Holdnack, J. A., Xiaobin Zhou, Larrabee, G. J., Millis, S. R., & Salthouse, T. A. (2011). Confirmatory factor analysis of the WAIS-IV/WMS-IV. *Assessment*, *18*(2), 178–191.

Horecka, K. M., Dulas, M. R., Schwarb, H., Lucas, H. D., Duff, M., & Cohen, N. J. (2018). Reconstructing relational information. *Hippocampus*, *28*(2), 164–177.

Hoscheidt, S. M., Nadel, L., Payne, J., & Ryan, L. (2010). Hippocampal activation during retrieval of spatial context from episodic and semantic memory. *Behavioural Brain Research*, *212*(2), 121–132.

Hrybouski, S., Aghamohammadi-Sereshki, A., Madan, C. R., Shafer, A. T., Baron, C. A., Seres, P., Beaulieu, C., Olsen, F., & Malykhin, N. V. (2016). Amygdala subnuclei response and connectivity during emotional processing. *NeuroImage*, *133*, 98–110.

Huang, Y., Coupland, N. J., Lebel, R. M., Carter, R., Seres, P., Wilman, A. H., & Malykhin, N. V. (2013). Structural changes in hippocampal subfields in major depressive disorder: a high-field magnetic resonance imaging study. *Biological Psychiatry*, *74*(1), 62–68.

Iglesias, J. E., Augustinack, J. C., Nguyen, K., Player, C. M., Player, A., Wright, M., Roy, N., Frosch, M. P., McKee, A. C., Wald, L. L., Fischl, B., & Leemput, K. V. (2015). A computational atlas of the hippocampal formation using ex vivo, ultra-high resolution MRI: Application to adaptive segmentation of in vivo MRI. *NeuroImage*, *115*, 117–137.

Jones, M. W., & McHugh, T. J. (2011). Updating hippocampal representations: CA2 joins the circuit. *Trends in Neurosciences*, *34*(10), 526–535.

Kensinger, E. A., & Corkin, S. (2004). Two routes to emotional memory: distinct neural processes for valence and arousal. *Proceedings of the National Academy of Sciences of the United States of America*, *101*(9), 3310–3315.

Kensinger, E. A. (2009). Remembering the Details: Effects of Emotion. *Emotion Review*, *1*(2), 99–113.

Kessels, R. P. C., Jaap Kappelle, L., de Haan, E. H. F., & Postma, A. (2002). Lateralization of spatial-memory processes: evidence on spatial span, maze learning, and memory for object locations. *Neuropsychologia*, *40*(8), 1465–1473.

Kim, H. (2015). Encoding and retrieval along the long axis of the hippocampus and their relationships with dorsal attention and default mode networks: The HERNET model. *Hippocampus*, *25*(4), 500–510.

Konkel, A., Warren, D. E., Duff, M. C., Tranel, D. N., & Cohen, N. J. (2008). Hippocampal amnesia impairs all manner of relational memory. *Frontiers in Human Neuroscience*, *2*, 15.

Kumaran, D., & Maguire, E. A. (2005). The human hippocampus: cognitive maps or relational memory? *The Journal of Neuroscience*, *25*(31), 7254–7259.

Kyle, C. T., Smuda, D. N., Hassan, A. S., & Ekstrom, A. D. (2015). Roles of human hippocampal subfields in retrieval of spatial and temporal context. *Behavioural Brain Research*, *278*, 549–558.

La Joie, R., Fouquet, M., Mézenge, F., Landeau, B., Villain, N., Mevel, K., Pélerin, A., Eustache, F., Desgranges, B., & Chételat, G. (2010). Differential effect of age on hippocampal subfields assessed using a new high-resolution 3T MR sequence. *NeuroImage*, *53*(2), 506–514.

Lacy, J. W., Yassa, M. A., Stark, S. M., Muftuler, L. T., & Stark, C. E. L. (2011). Distinct pattern separation related transfer functions in human CA3/dentate and CA1 revealed using high-resolution fMRI and variable mnemonic similarity. *Learning & Memory*, *18*(1), 15–18.

Leal, S. L., Noche, J. A., Murray, E. A., & Yassa, M. A. (2017). Disruption of amygdala-entorhinal-hippocampal network in late-life depression. *Hippocampus*, *27*(4), 464–476.

Lee, A. C. H., Barense, M. D., & Graham, K. S. (2005). The contribution of the human medial temporal lobe to perception: bridging the gap between animal and human studies. *The Quarterly Journal of Experimental Psychology. B, Comparative and Physiological Psychology*, *58*(3-4), 300–325.

Lepage, M., Habib, R., & Tulving, E. (1998). Hippocampal PET activations of memory encoding and retrieval: the HIPER model. *Hippocampus*, *8*(4), 313–322.

Lindberg, O., Walterfang, M., Looi, J. C. L., Malykhin, N., Östberg, P., Zandbelt, B., Styner, M., Paniagua, B., Velakoulis, D., Örndahl, E., & Wahlund, L.-O. (2012). Hippocampal shape analysis in Alzheimer's disease and frontotemporal lobar degeneration subtypes. *Journal of Alzheimer's Disease*, *30*(2), 355–365.

Lindquist, M. A., Meng Loh, J., Atlas, L. Y., & Wager, T. D. (2009). Modeling the hemodynamic response function in fMRI: efficiency, bias and mis-modeling. *NeuroImage*, *45*(1 Suppl), S187–98.

Lisman, J., Buzsáki, G., Eichenbaum, H., Nadel, L., Ranganath, C., & Redish, A. D. (2017). Viewpoints: how the hippocampus contributes to memory, navigation and cognition. *Nature Neuroscience*, *20*(11), 1434–1447.

Lisman, J. E., & Grace, A. A. (2005). The hippocampal-VTA loop: controlling the entry of information into long-term memory. *Neuron*, *46*(5), 703–713.

Logothetis, N. K., Pauls, J., Augath, M., Trinath, T., & Oeltermann, A. (2001). Neurophysiological investigation of the basis of the fMRI signal. *Nature*, *412*(6843), 150–157.

Madan, C. R., Fujiwara, E., Caplan, J. B., & Sommer, T. (2017). Emotional arousal impairs association-memory: Roles of amygdala and hippocampus. *NeuroImage*, *156*, 14–28.

Maller, J. J., Daskalakis, Z. J., & Fitzgerald, P. B. (2007). Hippocampal volumetrics in depression: the importance of the posterior tail. *Hippocampus*, *17*(11), 1023–1027.

Maller, J. J., Daskalakis, Z. J., Thomson, R. H. S., Daigle, M., Barr, M. S., & Fitzgerald, P. B. (2012). Hippocampal volumetrics in treatment-resistant depression and schizophrenia: the devil's in de-tail. *Hippocampus*, *22*(1), 9–16.

Maguire, E. A., Gadian, D. G., Johnsrude, I. S., Good, C. D., Ashburner, J., Frackowiak, R. S., & Frith, C. D. (2000). Navigation-related structural change in the hippocampi of taxi drivers. *Proceedings of the National Academy of Sciences of the United States of America*, *97*(8), 4398–4403.

Maguire, E. A., Spiers, H. J., Good, C. D., Hartley, T., Frackowiak, R. S. J., & Burgess, N. (2003). Navigation expertise and the human hippocampus: a structural brain imaging analysis. *Hippocampus*, *13*(2), 250–259.

Malykhin, N. V., Bouchard, T. P., Ogilvie, C. J., Coupland, N. J., Seres, P., & Camicioli, R. (2007). Three-dimensional volumetric analysis and reconstruction of amygdala and hippocampal head, body and tail. *Psychiatry Research*, *155*(2), 155–165.

Malykhin, N. V., Lebel, R. M., Coupland, N. J., Wilman, A. H., & Carter, R. (2010). In vivo quantification of hippocampal subfields using 4.7 T fast spin echo imaging. *NeuroImage*, *49*(2), 1224–1230.

Malykhin, N. V., Huang, Y., Hrybouski, S., & Olsen, F. (2017). Differential vulnerability of hippocampal subfields and anteroposterior hippocampal subregions in healthy cognitive aging. *Neurobiology of Aging*, *59*, 121–134.

Martin, P. K., & Schroeder, R. W. (2014). Chance performance and floor effects: threats to the validity of the Wechsler Memory Scale−fourth edition designs subtest. *Archives of Clinical Neuropsychology*, *29*(4), 385–390.

Meeter, M., Murre, J. M. J., & Talamini, L. M. (2004). Mode shifting between storage and recall based on novelty detection in oscillating hippocampal circuits. *Hippocampus*, *14*(6), 722–741.

Moscovitch, M., Cabeza, R., Winocur, G., & Nadel, L. (2016). Episodic memory and beyond: the hippocampus and neocortex in transformation. *Annual Review of Psychology*, *67*, 105–134.

Moscovitch, M., Rosenbaum, R. S., Gilboa, A., Addis, D. R., Westmacott, R., Grady, C., et al. (2005). Functional neuroanatomy of remote episodic, semantic and spatial memory: a unified account based on multiple trace theory. *Journal of Anatomy*, *207*(1), 35–66.

Murray, E. A., Bussey, T. J., & Saksida, L. M. (2007). Visual perception and memory: a new view of medial temporal lobe function in primates and rodents. *Neuroscience*, *30*, 99–122.

Nadel, L., Hupbach, A., Gomez, R., & Newman-Smith, K. (2012). Memory formation, consolidation and transformation. *Neuroscience and Biobehavioral Reviews*, *36*(7), 1640–1645.

Nauer, R. K., Whiteman, A. S., Dunne, M. F., Stern, C. E., & Schon, K. (2015). Hippocampal subfield and medial temporal cortical persistent activity during working memory reflects ongoing encoding. *Frontiers in Systems Neuroscience*, *9*, 30.

Nelder, J. A., & Mead, R. (1965). A Simplex Method for Function Minimization. *The Computer Journal*, *7*(4), 308–313.

Norman, K. A., & O'Reilly, R. C. (2003). Modeling hippocampal and neocortical contributions to recognition memory: a complementary-learning-systems approach. *Psychological Review*, *110*(4), 611–646.

Olman, C. A., Davachi, L., & Inati, S. (2009). Distortion and signal loss in medial temporal lobe. *PloS One*, *4*(12), e8160.

O'Keefe, J., & Nadel, L. (1978). *The hippocampus as a cognitive map*. Oxford: Clarendon Press.

O'Mara, S. (2006). Controlling hippocampal output: the central role of subiculum in hippocampal information processing. *Behavioural Brain Research*, *174*(2), 304–312.

O'Neil, E. B., Newsome, R. N., Li, I. H. N., Thavabalasingam, S., Ito, R., & Lee, A. C. H. (2015). Examining the Role of the Human Hippocampus in Approach-Avoidance Decision Making Using a Novel Conflict Paradigm and Multivariate Functional Magnetic Resonance Imaging. *Journal of Neuroscience*, *35*(45), 15039–15049.

Owen, A. M., Milner, B., Petrides, M., & Evans, A. C. (1996). A specific role for the right parahippocampal gyrus in the retrieval of object-location: a positron emission tomography study. *Journal of Cognitive Neuroscience*, *8*(6), 588–602.

Peirce, J. W. (2007). PsychoPy–Psychophysics software in Python. *Journal of Neuroscience Methods*, *162*(1–2), 8–13.

Peirce, J. W. (2009). Generating Stimuli for Neuroscience Using PsychoPy. *Frontiers in Neuroinformatics*, *2*, 10.

Perlbarg, V., Bellec, P., Anton, J.-L., Pélégrini-Issac, M., Doyon, J., & Benali, H. (2007). CORSICA: correction of structured noise in fMRI by automatic identification of ICA components. *Magnetic Resonance Imaging*, *25*(1), 35–46.

Pentkowski, N. S., Blanchard, D. C., Lever, C., Litvin, Y., & Blanchard, R. J. (2006). Effects of lesions to the dorsal and ventral hippocampus on defensive behaviors in rats. *The European Journal of Neuroscience*, *23*(8), 2185–2196.

Pernet, C. R. (2014). Misconceptions in the use of the General Linear Model applied to functional MRI: a tutorial for junior neuro-imagers. *Frontiers in Neuroscience*, *8*, 1.

Poppenk, J., Evensmoen, H. R., Moscovitch, M., & Nadel, L. (2013). Long-axis specialization of the human hippocampus. *Trends in Cognitive Sciences*, *17*(5), 230–240.

Poppenk, J., & Moscovitch, M. (2011). A hippocampal marker of recollection memory ability among healthy young adults: contributions of posterior and anterior segments. *Neuron*, *72*(6), 931–937.

Poppenk, J., Walia, G., McIntosh, A. R., Joanisse, M. F., Klein, D., & Köhler, S. (2008). Why is the meaning of a sentence better remembered than its form? An fMRI study on the role of novelty-encoding processes. *Hippocampus*, *18*(9), 909–918.

Postma, A., Kessels, R. P. C., & van Asselen, M. (2008). How the brain remembers and forgets where things are: the neurocognition of object-location memory. *Neuroscience and Biobehavioral Reviews*, *32*(8), 1339–1345.

Preston, A. R., Bornstein, A. M., Hutchinson, J. B., Gaare, M. E., Glover, G. H., & Wagner, A. D. (2010). High-resolution fMRI of content-sensitive subsequent memory responses in human medial temporal lobe. *Journal of Cognitive Neuroscience*, *22*(1), 156–173.

Pruessner, J. C., Li, L. M., Serles, W., Pruessner, M., Collins, D. L., Kabani, N., Lupien, S., & Evans, A. C. (2000). Volumetry of hippocampus and amygdala with high-resolution MRI and three-dimensional analysis software: minimizing the discrepancies between laboratories. *Cerebral Cortex*, *10*(4), 433–442.

Rajah, M. N., Kromas, M., Han, J. E., & Pruessner, J. C. (2010). Group differences in anterior hippocampal volume and in the retrieval of spatial and temporal context memory in healthy young versus older adults. *Neuropsychologia*, *48*(14), 4020–4030.

Ranganath, C., & Ritchey, M. (2012). Two cortical systems for memory-guided behaviour. *Nature Reviews. Neuroscience*, *13*(10), 713–726.

Ranganath, C., Yonelinas, A. P., Cohen, M. X., Dy, C. J., Tom, S. M., & D'Esposito, M. (2004). Dissociable correlates of recollection and familiarity within the medial temporal lobes. *Neuropsychologia*, *42*(1), 2–13.

Reagh, Z. M., Watabe, J., Ly, M., Murray, E., & Yassa, M. A. (2014). Dissociated signals in human dentate gyrus and CA3 predict different facets of recognition memory. *Journal of Neuroscience*, *34*(40), 13301–13313.

Rössler, M., Zarski, R., Bohl, J., & Ohm, T. G. (2002). Stage-dependent and sector-specific neuronal loss in hippocampus during Alzheimer's disease. *Acta Neuropathologica*, *103*(4), 363–369.

Roy, D. S., Kitamura, T., Okuyama, T., Ogawa, S. K., Sun, C., Obata, Y., et al. (2017). Distinct Neural Circuits for the Formation and Retrieval of Episodic Memories. *Cell*, *170*(5), 1000–1012.e19.

Rummel, C., Verma, R. K., Schoepf, V., Abela, E., Hauf, M., Zapata Berruecos, J. F., & Wiest, R. (2013). Time course based artifact identification for independent components of resting-state fMRI. *Frontiers in Human Neuroscience*, *7*.

Ryan, L., Lin, C.-Y., Ketcham, K., & Nadel, L. (2010). The role of medial temporal lobe in retrieving spatial and nonspatial relations from episodic and semantic memory. *Hippocampus*, *20*(1), 11–18.

Salimi-Khorshidi, G., Douaud, G., Beckmann, C. F., Glasser, M. F., Griffanti, L., & Smith, S. M. (2014). Automatic denoising of functional MRI data: combining independent component analysis and hierarchical fusion of classifiers. *NeuroImage*, *90*, 449–468.

Schacter, D. L., Curran, T., Reiman, E. M., Chen, K., Bandy, D. J., & Frost, J. T. (1999). Medial temporal lobe activation during episodic encoding and retrieval: a PET study. *Hippocampus*, *9*(5), 575–581.

Schacter, D. L., & Wagner, A. D. (1999). Medial temporal lobe activations in fMRI and PET studies of episodic encoding and retrieval. *Hippocampus*, *9*(1), 7–24.

Scoville, W. B., & Milner, B. (1957). Loss of recent memory after bilateral hippocampal lesions. *Journal of Neurology, Neurosurgery, and Psychiatry*, *20*(1), 11–21.

Shmuel, A., Augath, M., Oeltermann, A., & Logothetis, N. K. (2006). Negative functional MRI response correlates with decreases in neuronal activity in monkey visual area V1. *Nature Neuroscience*, *9*(4), 569–577.

Simić, G., Kostović, I., Winblad, B., & Bogdanović, N. (1997). Volume and number of neurons of the human hippocampal formation in normal aging and Alzheimer's disease. *Journal of Comparative Neurology*, *379*(4), 482–494.

Sled, J. G., Zijdenbos, A. P., & Evans, A. C. (1998). A nonparametric method for automatic correction of intensity nonuniformity in MRI data. *IEEE Transactions on Medical Imaging*, *17*(1), 87–97.

Small, S. A. (2002). The longitudinal axis of the hippocampal formation: its anatomy, circuitry, and role in cognitive function. *Reviews in the Neurosciences*, *13*(2), 183–194.

Smith, M. L., & Milner, B. (1981). The role of the right hippocampus in the recall of spatial location. *Neuropsychologia*, *19*(6), 781–793.

Spalletta, G., Cravello, L., Gianni, W., Piras, F., Iorio, M., Cacciari, C., Casini, A. R., Chiapponi, C., Sancesario, G., Fratangeli, C., Orfei, M. D., Caltagirone, C., & Piras F. (2016). Homotaurine effects on hippocampal volume loss and episodic memory in amnestic mild cognitive impairment. *Journal of Alzheimer's Disease*, *50*(3), 807–816.

Spaniol, J., Davidson, P. S. R., Kim, A. S. N., Han, H., Moscovitch, M., & Grady, C. L. (2009). Event-related fMRI studies of episodic encoding and retrieval: meta-analyses using activation likelihood estimation. *Neuropsychologia*, *47*(8-9), 1765–1779.

Stark, C. E., & Squire, L. R. (2001). When zero is not zero: the problem of ambiguous baseline conditions in fMRI. *Proceedings of the National Academy of Sciences of the United States of America*, *98*(22), 12760–12766.

Storti, S. F., Formaggio, E., Nordio, R., Manganotti, P., Fiaschi, A., Bertoldo, A., & Toffolo, G. M. (2013). Automatic selection of resting-state networks with functional magnetic resonance imaging. *Frontiers in Neuroscience*, *7*, 72.

Strange, B. A., Witter, M. P., Lein, E. S., & Moser, E. I. (2014). Functional organization of the hippocampal longitudinal axis. *Nature Reviews. Neuroscience*, *15*(10), 655–669.

Stokes, J., Kyle, C., & Ekstrom, A. D. (2015). Complementary roles of human hippocampal subfields in differentiation and integration of spatial context. *Journal of Cognitive Neuroscience*, *27*(3), 546–559.

Squire, L. R., & Dede, A. J. O. (2015). Conscious and unconscious memory systems. *Cold Spring Harbor Perspectives in Biology*, *7*(3), a021667.

Squire, L. R., Genzel, L., Wixted, J. T., & Morris, R. G. (2015). Memory consolidation. *Cold Spring Harbor Perspectives in Biology*, *7*(8), a021766.

Squire, L. R., & Wixted, J. T. (2011). The cognitive neuroscience of human memory since H.M. *Annual Review of Neuroscience*, *34*, 259–288.

Suthana, N. A., Donix, M., Wozny, D. R., Bazih, A., Jones, M., Heidemann, R. M., Trampel, R., Ekstrom, A. D., Scharf, M., Knowlton, B., Turner, R., & Bookheimer, S. Y. (2015). High-resolution 7T fMRI of Human Hippocampal Subfields during Associative Learning. *Journal of Cognitive Neuroscience*, *27*(6), 1194–1206.

Suthana, N. A., Ekstrom, A. D., Moshirvaziri, S., Knowlton, B., & Bookheimer, S. Y. (2009). Human hippocampal CA1 involvement during allocentric encoding of spatial information. *The Journal of Neuroscience*, *29*(34), 10512–10519.

Suthana, N. A., Ekstrom, A. D., Moshirvaziri, S., Knowlton, B., & Bookheimer, S. Y. (2011). Dissociations within human hippocampal subregions during encoding and retrieval of spatial information. *Hippocampus*, *21*(7), 694–701.

Suzuki, W. A., & Baxter, M. G. (2009). Memory, perception, and the medial temporal lobe: a synthesis of opinions. *Neuron*, *61*(5), 678–679.

Tohka, J., Foerde, K., Aron, A. R., Tom, S. M., Toga, A. W., & Poldrack, R. A. (2008). Automatic independent component labeling for artifact removal in fMRI. *NeuroImage*, *39*, 1227–1245.

Tompary, A., Duncan, K., & Davachi, L. (2016). High-resolution investigation of memory-specific reinstatement in the hippocampus and perirhinal cortex. *Hippocampus*, *26*(8), 995–1007.

Travis, S. G., Huang, Y., Fujiwara, E., Radomski, A., Olsen, F., Carter, R., Seres, P., & Malykhin, N. V. (2014). High field structural MRI reveals specific episodic memory correlates in the subfields of the hippocampus. *Neuropsychologia*, *53*, 233–245.

de Vanssay-Maigne, A., Noulhiane, M., Devauchelle, A. D., Rodrigo, S., Baudoin-Chial, S., Meder, J. F., et al. (2011). Modulation of encoding and retrieval by recollection and familiarity: Mapping the medial temporal lobe networks. *NeuroImage*, *58*(4), 1131–1138.

van Asselen, M., Kessels, R. P. C., Kappelle, L. J., & Postma, A. (2008). Categorical and coordinate spatial representations within object-location memory. *Cortex*, *44*(3), 249–256.

Vassilopoulou, K., Papathanasiou, M., Michopoulos, I., Boufidou, F., Oulis, P., Kelekis, N., et al. (2013). A magnetic resonance imaging study of hippocampal, amygdala and subgenual prefrontal cortex volumes in major depression subtypes: melancholic versus psychotic depression. *Journal of Affective Disorders*, *146*(2), 197–204.

Vinogradova, O. S. (2001). Hippocampus as comparator: role of the two input and two output systems of the hippocampus in selection and registration of information. *Hippocampus*, *11*(5), 578–598.

Watson, P. D., Voss, J. L., Warren, D. E., Tranel, D., & Cohen, N. J. (2013). Spatial reconstruction by patients with hippocampal damage is dominated by relational memory errors. *Hippocampus*, *23*(7), 570–580.

Wechsler, D. (2009). Wechsler Memory Scale-IV administration and scoring manual. San Antonio, TX: Pearson.

Whitfield-Gabrieli, S., & Nieto-Castanon, A. (2012). Conn: a functional connectivity toolbox for correlated and anticorrelated brain networks. *Brain Connectivity*, *2*(3), 125–141.

Winterburn, J. L., Pruessner, J. C., Chavez, S., Schira, M. M., Lobaugh, N. J., Voineskos, A. N., & Chakravarty, M. M. (2013). A novel in vivo atlas of human hippocampal subfields using high-resolution 3 T magnetic resonance imaging. *NeuroImage*, *74*, 254–265.

Wisse, L. E. M., Gerritsen, L., Zwanenburg, J. J. M., Kuijf, H. J., Luijten, P. R., Biessels, G. J., & Geerlings, M. I. (2012). Subfields of the hippocampal formation at 7 T MRI: in vivo volumetric assessment. *NeuroImage*, *61*(4), 1043–1049.

Woollett, K., & Maguire, E. A. (2009). Navigational expertise may compromise anterograde associative memory. *Neuropsychologia*, *47*(4), 1088–1095.

Woollett, K., & Maguire, E. A. (2011). Acquiring "the Knowledge" of London's layout drives structural brain changes. *Current Biology*, *21*(24), 2109–2114.

Woollett, K., & Maguire, E. A. (2012). Exploring anterograde associative memory in London taxi drivers. *Neuroreport*, *23*(15), 885–888.

Woollett, K., Spiers, H. J., & Maguire, E. A. (2009). Talent in the taxi: a model system for exploring expertise. *Philosophical Transactions of the Royal Society of London. Series B, Biological Sciences*, *364*(1522), 1407–1416.

Yassa, M. A., Mattfeld, A. T., Stark, S. M., & Stark, C. E. L. (2011). Age-related memory deficits linked to circuit-specific disruptions in the hippocampus. *Proceedings of the National Academy of Sciences of the United States of America*, *108*(21), 8873–8878.

Yassa, M. A., & Stark, C. E. L. (2011). Pattern separation in the hippocampus. *Trends in Neurosciences*, *34*(10), 515–525.

Yushkevich, P.A., Amaral, R.S., Augustinack, J.C., Bender, A.R., Bernstein, J.D., Boccardi, M., Bocchetta, M., Burggren, A.C., Carr, V.A., Chakravarty, M.M., Chételat, G., Daugherty, A.M., Davachi, L., Ding, S.L., Ekstrom, A., Geerlings, M.I., Hassan, A., Huang, Y., Iglesias, J.E., La Joie, R., Kerchner, G.A., LaRocque, K.F., Libby, L.A., Malykhin, N., Mueller, S.G., Olsen, R.K., Palombo, D.J., Parekh, M.B., Pluta, J.B., Preston, A.R., Pruessner, J.C., Ranganath, C., Raz, N., Schlichting, M.L., Schoemaker, D., Singh, S., Stark, C.E., Suthana, N., Tompary, A., Turowski, M.M., Van Leemput, K., Wagner, A.D., Wang, L., Winterburn, J.L., Wisse, L.E., Yassa, M.A., Zeineh, M.M. (2015a). Quantitative comparison of 21 protocols for labeling hippocampal subfields and parahippocampal subregions in in vivo MRI: Towards a harmonized segmentation protocol. *NeuroImage*, *111*, 526–541.

Yushkevich, P. A., Pluta, J. B., Wang, H., Xie, L., Ding, S.-L., Gertje, E. C., Mancuso, L., Kliot, D., Das, S. R., & Wolk, D. A. (2015b). Automated volumetry and regional thickness analysis of hippocampal subfields and medial temporal cortical structures in mild cognitive impairment. *Human Brain Mapping*, *36*(1), 258–287.

Yushkevich, P.A., Piven, J., Hazlett, H. C., Smith, R. G., Ho, S., Gee, J. C., & Ceric, G. (2006). User-guided 3D active contour segmentation of anatomical structures: significantly improved efficiency and reliability. *NeuroImage*, *31*(3), 1116–1128.

Zeidman, P., & Maguire, E. A. (2016). Anterior hippocampus: the anatomy of perception, imagination and episodic memory. *Nature Reviews. Neuroscience*, *17*(3), 173–182.

Zeidman, P., Lutti, A., & Maguire, E. A. (2015). Investigating the functions of subregions within anterior hippocampus. *Cortex*, *73*, 240–256.

Zeineh, M. M., Engel, S. A., Thompson, P. M., & Bookheimer, S. Y. (2003). Dynamics of the hippocampus during encoding and retrieval of face-name pairs. *Science*, *299*(5606), 577–580.

Table 1. Number of voxels for each of the HC subregion and subfield ROIs. Values are in raw fMRI (1.5-mm isotropic) voxel counts, averaged across participants.

Subregion/Subfield (voxel count ± SD)	*Cornu Ammonis* 1-3		Dentate Gyrus		Subiculum		Total HC Subregions	
	Left	Right	Left	Right	Left	Right	Left	Right
HC Head	317.8 ± 72.0	359.8 ± 85.1	94.7 ± 16.4	102.9 ± 11.3	131.6 ± 30.5	135.6 ± 33.5	544.1 ± 99.2	598.2 ± 112.8
HC Body	110.0 ± 23.7	122.6 ± 15.8	147.8 ± 23.7	148.6 ± 20.1	105.0 ± 20.1	109.1 ± 20.3	362.8 ± 48.4	380.2 ± 41.3
HC Tail	63.8 ± 12.0	63.3 ± 17.3	106.2 ± 29.0	110.8 ± 30.2	13.0 ± 6.4	14.5 ± 7.2	183.0 ± 41.0	188.6 ± 41.1
HC Body + Tail	173.9 ± 29.5	185.9 ± 24.0	254.0 ± 42.4	259.4 ± 42.8	118.1 ± 22.6	123.4 ± 22.2	545.8 ± 72.5	568.8 ± 66.4
Total HC Subfields	491.7 ± 74.5	545.6 ± 84.2	348.7 ± 46.2	362.3 ± 45.7	249.7 ± 41.8	259.2 ± 46.7	1090.0 ± 108.6	1155.6 ± 113.3

Table 2. Effective temporal signal-to-noise (tSNR) ratios for each HC ROI. All SNR values were computed on preprocessed data (motion correction, despiking, and accounting for non-BOLD cardiac- and pulmonary- related waveforms). The upper half of the table shows ROI-level tSNR, computed from voxel-averaged time series across the entire ROI. The bottom half of the table shows average voxelwise tSNR. Here, tSNR was computed for each HC voxel, without averaging time series across voxels, and resulting tSNR values were averaged across ROI voxels.

| Subregion/ Subfield	Cornu Ammonis 1-3		Dentate Gyrus		Subiculum		Total HC Subregions	
	Left	Right	Left	Right	Left	Right	Left	Right
ROI tSNR ± SD								
HC Head	285.5 ± 42.0	344.6 ± 37.4	176.7 ± 37.6	215.6 ± 35.2	201.9 ± 26.4	229.1 ± 39.3	324.8 ± 41.6	385.6 ± 42.3
HC Body	202.5 ± 44.4	278.0 ± 49.8	218.4 ± 41.0	261.9 ± 40.1	215.6 ± 40.5	259.9 ± 39.7	300.2 ± 50.3	371.1 ± 48.9
HC Tail	213.4 ± 45.1	261.5 ± 46.3	252.7 ± 50.5	284.8 ± 48.0	115.2 ± 29.6	136.9 ± 34.2	305.5 ± 53.4	348.8 ± 48.6
HC Body + Tail	272.1 ± 55.2	352.2 ± 52.3	296.0 ± 47.7	342.4 ± 47.7	232.2 ± 41.7	276.6 ± 39.8	374.7 ± 56.2	443.4 ± 47.2
Total HC Subfields	360.4 ± 52.4	450.2 ± 48.2	319.4 ± 46.7	370.7 ± 45.8	290.2 ± 29.6	342.2 ± 40.2	423.7 ± 58.3	516.4 ± 50.6
Voxel tSNR ± SD								
HC Head	36.0 ± 6.7	38.9 ± 7.7	35.1 ± 7.7	41.1 ± 8.3	33.3 ± 6.0	35.9 ± 6.9	35.2 ± 6.6	38.6 ± 7.6
HC Body	33.2 ± 7.3	44.2 ± 7.6	36.2 ± 7.6	44.8 ± 7.5	35.9 ± 7.0	42.4 ± 6.4	35.2 ± 7.2	43.9 ± 7.2
HC Tail	45.9 ± 7.6	52.3 ± 6.6	47.0 ± 7.3	52.2 ± 7.0	44.6 ± 6.8	49.2 ± 6.7	46.4 ± 7.3	52.1 ± 6.8
HC Body + Tail	37.9 ± 7.4	47.0 ± 7.0	40.7 ± 7.4	48.0 ± 7.0	36.9 ± 6.9	42.9 ± 6.2	39.0 ± 7.3	46.6 ± 6.8
Total HC Subfields	36.6 ± 6.7	41.7 ± 7.6	39.2 ± 7.3	46.0 ± 7.2	35.0 ± 6.2	39.4 ± 6.5	37.1 ± 6.8	42.4 ± 7.5

Table 3. Summary of main results.

|	encoding		retrieval		encoding – retrieval	
	relative to zero	differences	relative to zero	differences	relative to zero	differences
total hippocampus						
left	↑ 0.23% [d = 1.60] ***	left > right [d = 0.39] ~	↓ 0.18% [d = 0.64] * (location trials only)	right > left 0.25% [d = 1.11] *** on location trials only	0.26% [d = 1.20] ***	left > right [d = 0.52] *
right	↑ 0.15% [d = 0.86] ***		↑ 0.05% [d = 0.40] ~ (all trials)		0.10% [d = 0.44] *	
bilateral total subfields (transverse axis)						
CA1-3	↑ 0.16% [d = 1.08] ***	DG > CA1-3 [d = 0.90] ***	↓ 0.06% [d = 0.47] ~	DG > CA1-3 [d = 1.15] ***	0.22% [d = 1.31] ***	CA1-3 > Sub [d = 0.55] *
DG	↑ 0.29% [d = 1.91] ***	DG > Sub [d = 1.03] ***	↑ 0.10% [d = 0.93] ***	DG > Sub [d = 0.58] *	0.18% [d = 0.88] ***	DG > Sub [d = 0.46] ~
Sub	↑ 0.11% [d = 0.64] **		↑ 0.02% [d = 0.11], n.s.		0.09% [d = 0.40] ~	
bilateral subregions (longitudinal axis)						
head	↑ 0.16% [d = 0.70] **	head < body < tail linear gradient for location trials only (p = .025); no other differences	↓ 0.12% [d = 0.86] ***	head < body < tail linear gradient, regardless of memory type	0.27% [d = 1.24] ***	head > body [0.17%, d = 0.74] ** head > tail [0.20%, d = 0.54] *
body	↑ 0.21% [d = 1.54] ***		↑ 0.11% [d = 0.78] ***		posterior (i.e. body + tail): 0.10% [d = 0.62] *	
tail	↑ 0.26% [d = 1.61] ***		↑ 0.18% [d = 1.09] ***			
bilateral anterior (i.e., head) subfields						
CA1-3	↑ 0.15% [d = 0.56] *	none	↓ 0.14% [d = 0.80] **	none	0.29% [d = 1.10] ***	none
DG	↑ 0.19% [d = 0.69] **		↓ 0.09% [d = 0.46] ~		0.28% [d = 0.96] ***	
Sub	↑ 0.15% [d = 0.56] *		↓ 0.06% [d = 0.32], n.s.		0.21% [d = 0.66] **	
bilateral posterior (i.e., body + tail) subfields						
CA1-3	↑ 0.20% [d = 1.49] ***	DG > CA1-3 [d = 0.53] *	↑ 0.06% [d = 0.39] ~	DG > CA1-3 [d = 0.76] **	0.14% [d = 0.75] **	DG > Sub [d = 0.58] *
DG	↑ 0.31% [d = 1.85] ***	DG > Sub [d = 1.13] ***	↑ 0.18% [d = 1.51] ***	DG > Sub [d = 0.54] *	0.13% [d = 0.57] *	CA1-3 > Sub [d = 0.52] *
Sub	↑ 0.09% [d = 0.59] **	CA1-3 > Sub [d = 0.51] *	↑ 0.09% [d = 0.56] *		0.00% [d = 0.01], n.s.	
bilateral posterior – bilateral anterior subfields						
CA1-3	0.05% [d = 0.16], n.s.	none	0.20% [d = 0.92] ***	DG > Sub [d = 0.55] *	− 0.15% [d = 0.48] ~	none
DG	0.12% [d = 0.35], n.s.		0.27% [d = 1.30] ***		− 0.15% [d = 0.47] ~	
Sub	− 0.06% [d = 0.18], n.s.		0.15% [d = 0.75] ***		− 0.21% [d = 0.59] *	

~ FWE p < .10   * FWE p < .05   ** FWE p < .01   *** FWE p < .001
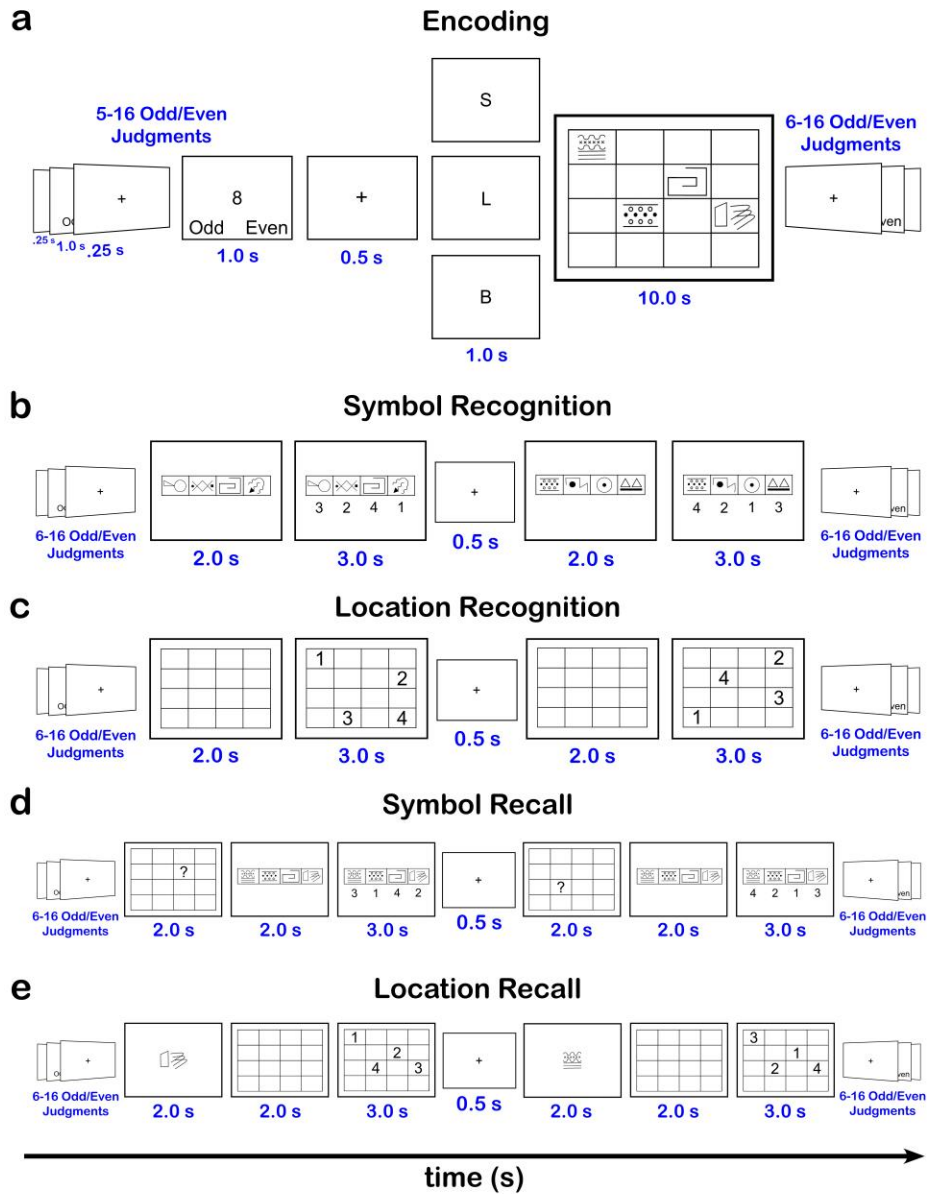
Figure 1. Computerized adaptation of the WMS-IV 'Designs' subtest that was used to study memory encoding (a) and memory retrieval (b-e) processes. Depending on encoding cue, memory was tested using one of the retrieval designs (b-e). An odd/even judgment task was used as a cognitive baseline, and separated trials from each other. See main text for detailed task description.
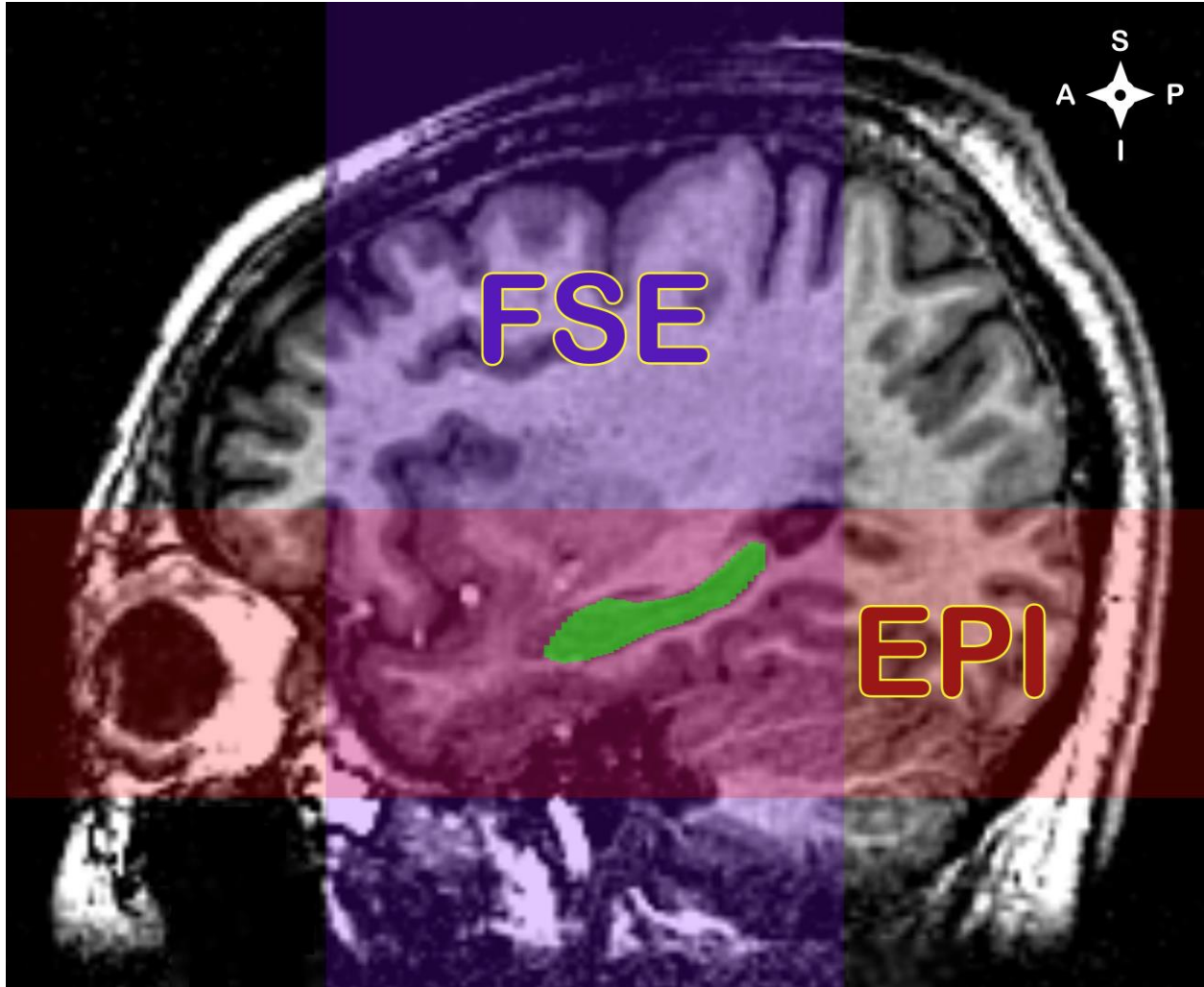
Figure 2. Brain tissue covered by high-resolution anatomical and high-resolution functional scans. Single participant's full-brain T1-weighted anatomical scan is shown in the background. Violet overlay represents coverage of ultra-high-resolution anatomical 2D FSE scan, which was used for manual segmentation of the hippocampal subfields and subregions. Red overlay represents areas captured by high-resolution fMRI EPI acquisition. Segmented hippocampus is shown in green.
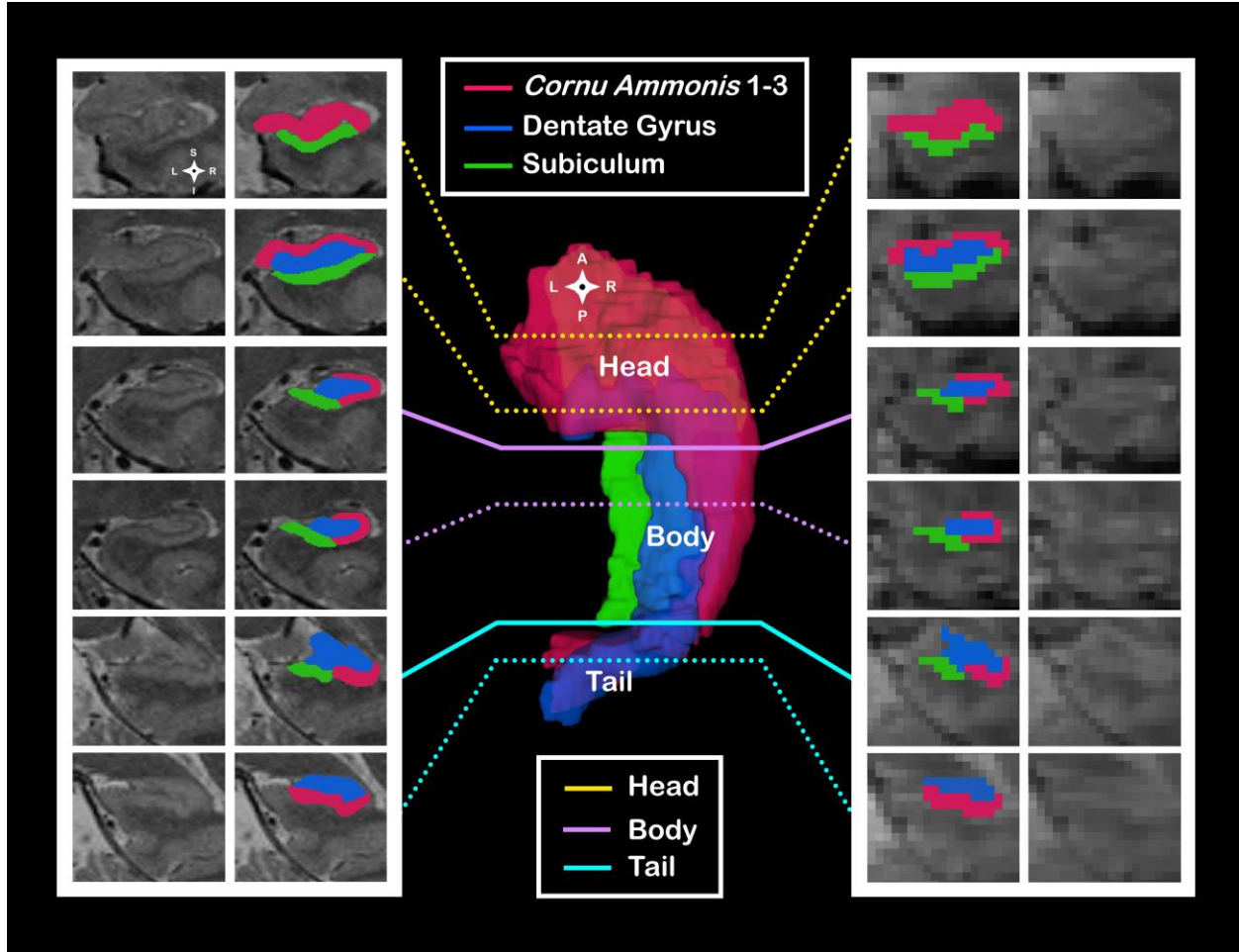
Figure 3. Three-dimensional reconstruction of the hippocampal subfields and anteroposterior subregions from a healthy volunteer. Panels to the left of the 3D model show subfield and subregions ROIs on a high-resolution T2-weighted structural scan. Panels to the right of the 3D reconstruction show subfield and subregion masks after they were registered and downsampled to fMRI resolution.
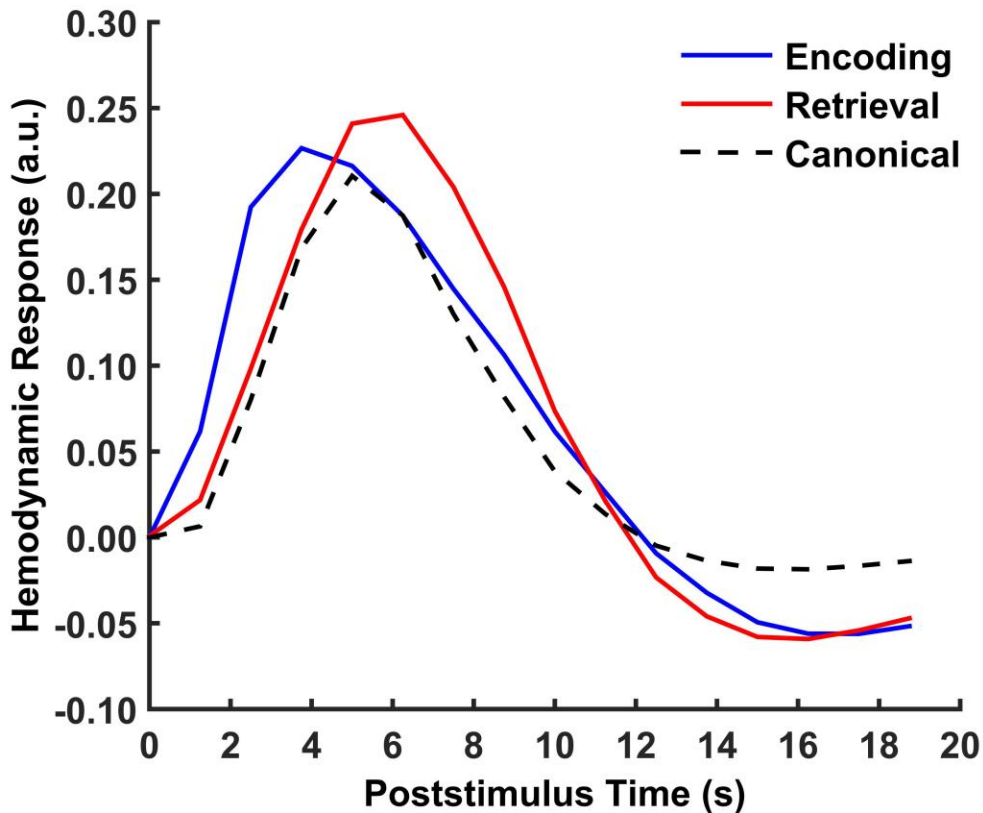
Figure 4. Fitted BOLD response functions for encoding and retrieval phases of our task, averaged across participants. Encoding and retrieval double-gamma functions were optimized to fit the hippocampal BOLD response, estimated using Finite Impulse Response and Informed Basis Set models (a.u., arbitrary units). Fitted Encoding/retrieval parameters were 6.01/11.98 for delay of response, 16.23/12.08 for delay of undershoot, 2.75/2.06 for dispersion of response, 1.35/2.06 for dispersion of undershoot, 2.19/1.01 for ratio of response to undershoot, and 0.69/-0.81 for onset.
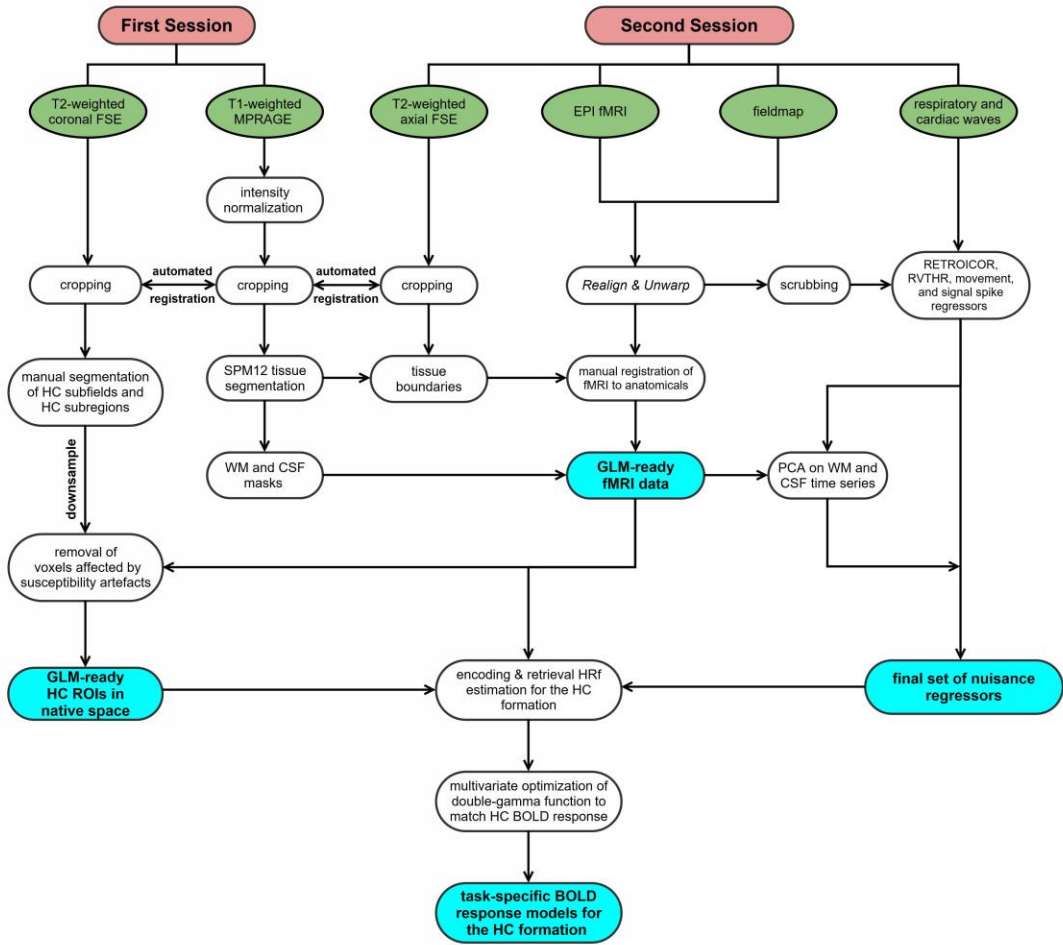
Figure 5. Schematic of the analysis pipeline. Green boxes represent raw data, and blue boxes represent final inputs into HC ROI activity analysis. See methods section for detailed description of each step.
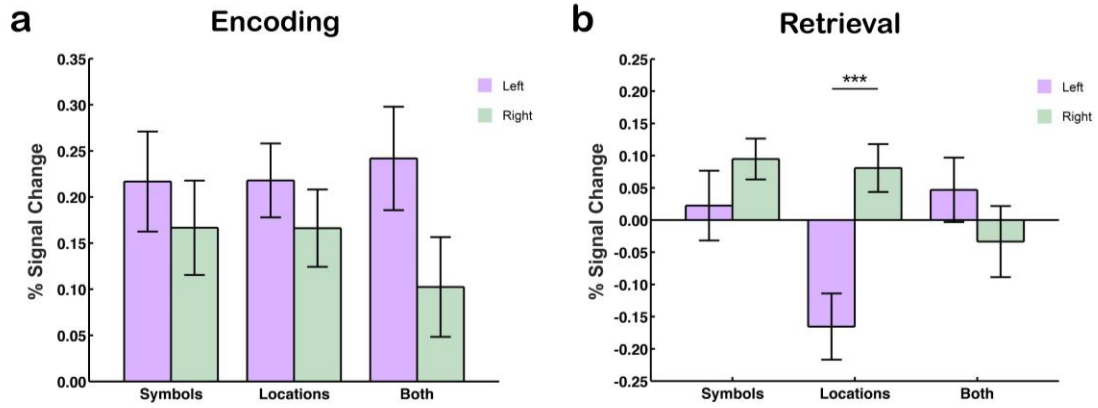
Figure 6. Activity in the total HC during the encoding (a) and retrieval (b) phases of our memory

task, separated by trial type and hemisphere. Error bars represent the standard error of the mean.

*** FWE $p < .001$.
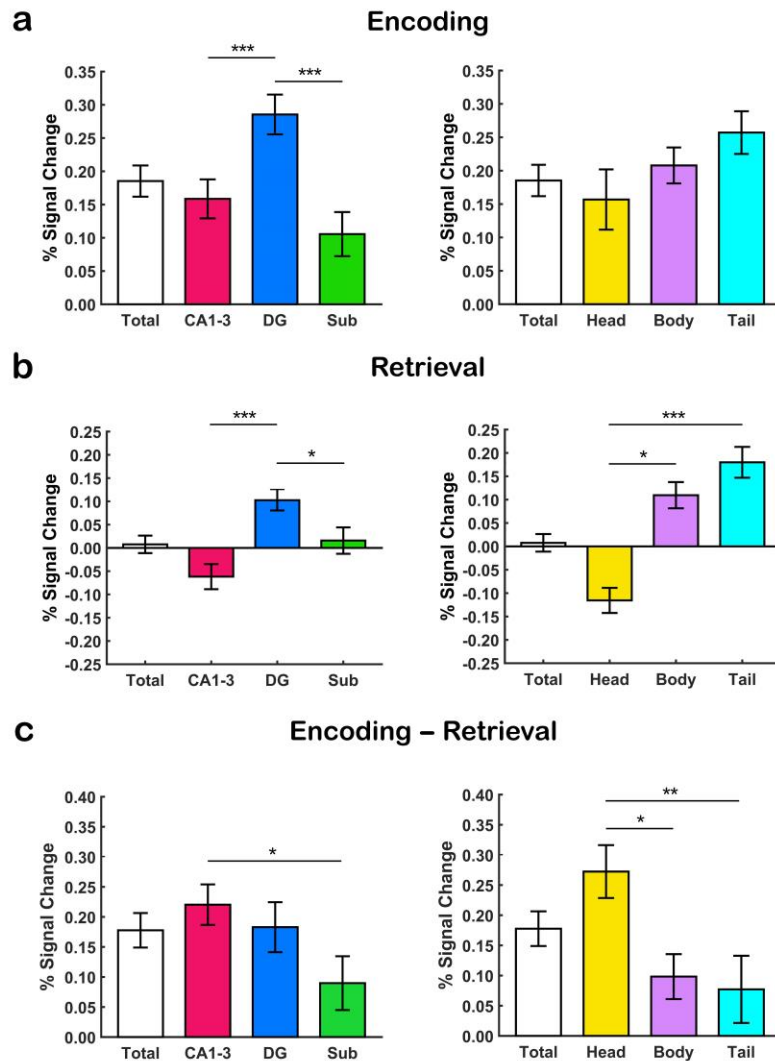
Figure 7. Activity in the total HC subfields and anteroposterior subregions during the encoding (a) and retrieval (b) phases, collapsed across symbol, location, and association trial types and both hemispheres. The bottom row (c) shows the encoding vs. retrieval BOLD activity differential. Abbreviations: CA1-3, *Cornu Ammonis* 1-3; DG, dentate gyrus; Sub, subiculum. Error bars represent the standard error of the mean. See main text for statistical comparisons vs. baseline. * FWE $p < .05$; ** FWE $p < .01$; *** FWE $p < .001$.
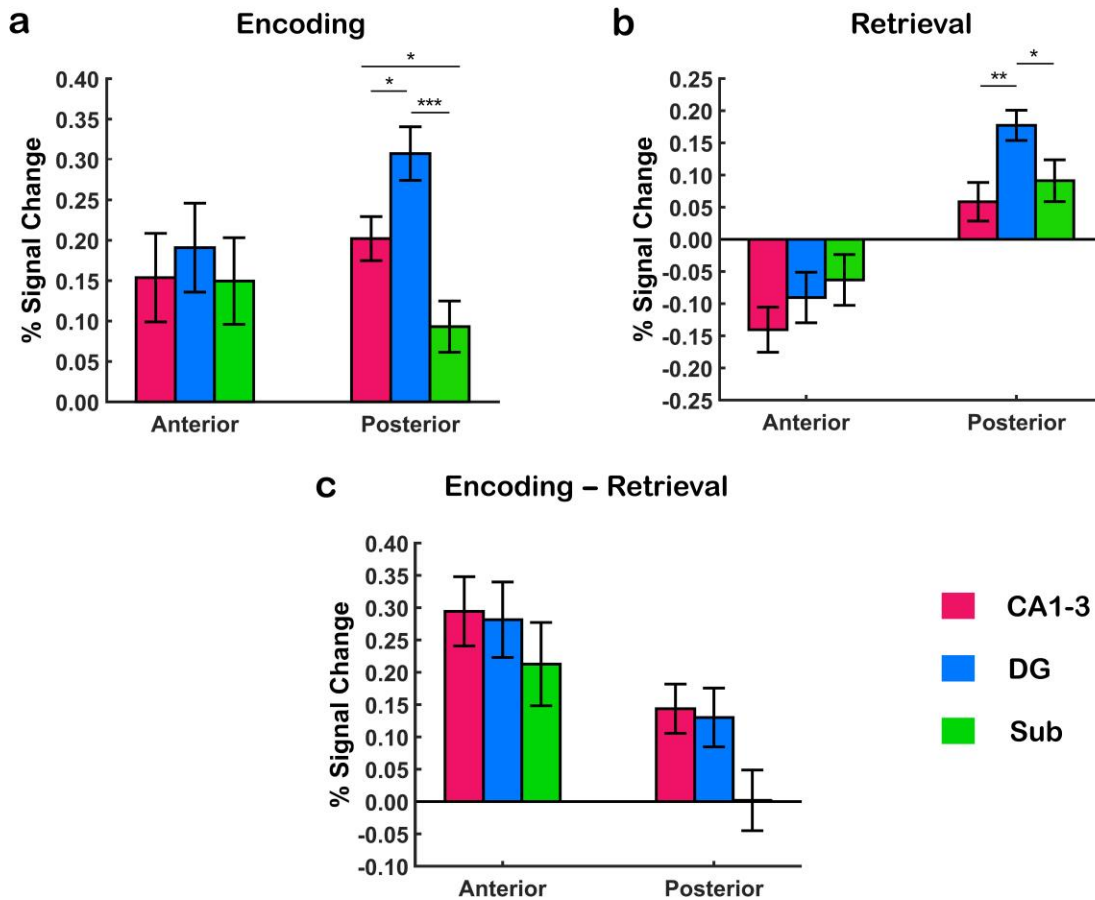
Figure 8. Estimated BOLD activity in the anterior (i.e., head) and posterior (i.e., body + tail) hippocampal subfields during memory encoding (a) and retrieval (b), collapsed across symbol, location, and association trial types and both hemispheres. The bottom panel (c) shows the encoding vs. retrieval BOLD activity differential for the anterior and posterior sections of the hippocampal subfields (CA1-3, *Cornu Ammonis* 1-3; DG, dentate gyrus; Sub, subiculum). Error bars represent the standard error of the mean. Only comparisons among subfields within, but not across, the anterior and posterior HC segments are shown. See main text for statistical comparisons between the anterior and posterior segments of each subfield, and for statistical comparisons vs. baseline. * FWE $p < .05$; ** FWE $p < .01$; *** FWE $p < .001$.